University of Nebraska Medical Center
DigitalCommons@UNMC

Theses & Dissertations | Graduate Studies

Summer 8-14-2020

Effect of Nanofiller Coating and Loading on Facial Elastomer Physical Properties

Rahmi K. Aulia
University of Nebraska Medical Center

Tell us how you used this information in this short survey.

Follow this and additional works at: https://digitalcommons.unmc.edu/etd

 Part of the Dental Materials Commons, Polymer and Organic Materials Commons, and the Prosthodontics and Prosthodontology Commons

Recommended Citation

Aulia, Rahmi K., "Effect of Nanofiller Coating and Loading on Facial Elastomer Physical Properties" (2020). *Theses & Dissertations*. 474.
https://digitalcommons.unmc.edu/etd/474

This Thesis is brought to you for free and open access by the Graduate Studies at DigitalCommons@UNMC. It has been accepted for inclusion in Theses & Dissertations by an authorized administrator of DigitalCommons@UNMC. For more information, please contact digitalcommons@unmc.edu.

EFFECT OF NANOFILLER COATING AND LOADING ON FACIAL ELASTOMER PHYSICAL PROPERTIES

by

Rahmi Khairani Aulia

A THESIS

Presented to the Faculty of
The University of Nebraska Graduate College
In Partial Fulfillment of the Requirements
For the Degree of Master of Science

Medical Sciences Interdepartmental Area
Graduate Program
Oral Biology

Under Supervision of Professor Mark W. Beatty

University of Nebraska Medical Center
Lincoln, Nebraska

July 2020

Advisory Committee:

James K. Wahl, III, Ph.D
Larry D. Crouch, Ph.D
Jennifer R. Keshwani, Ph.D

ACKNOWLEDGMENTS

By coming to the end of this journey; all praises to Allah SWT for giving me blessings, opportunity, determination, and strength to finish my study. In addition, may peace be given to Prophet Muhammad SAW, whose way of life has been continuous guidance.

I would like to express my deepest gratitude to my advisor, Dr. Mark Beatty, for his guidance since I became a graduate student. You have been a tremendous mentor for me. Your patience, enthusiasm, and immense knowledge helped me throughout the program, especially in the time of research and writing this thesis. I could not have imagined having a better advisor. You are my role model of becoming a teacher and researcher in the future.

I would also like to extend my sincere gratitude to my committee members: Dr. James Wahl III, Dr. Larry Crouch, and Dr. Jennifer Keshwani, for generously offering time, insights, and guidance throughout the process of this project.

I'm incredibly grateful to have Bobby Simetich as my Dental Biomaterial Lab mentor and my best friend. Thank you for all the sincere help throughout my study, which allows me to complete this thesis.

Many thanks to UNMC and the Fulbright Program for giving me this opportunity to receive a master's degree in the United States. This is my most exceptional experience, therefore, I'm forever grateful. Special thanks to my fellow Indonesian Fulbrighters 2018, as one of my great support systems in graduate life.

Finally, and most importantly, I would like to pay my special regards to my family. To my father and my brothers for always supporting me from afar. To my husband, for always being there for me (virtually), especially when I'm feeling down during my walk on this journey. And for my beloved late mother, this achievement is for you, Mama.

EFFECT OF FILLER COATING AND LOADING ON

FACIAL ELASTOMER PHYSICAL PROPERTIES

Rahmi K. Aulia, M.S

University of Nebraska, 2020

Advisor: Mark W. Beatty, D.D.S., M.S.E., M.S.D., M.S.

Current materials used for facial prostheses are far from being desirable, and improved properties with “skin-like” feel are needed. This study evaluates property changes induced by sequential additions of uncoated and hydrophobic-coated nano-SiO_2 to polydimethylsiloxane (PDMS) and compares them with those measured for conventional submicron SiO_2-filled materials. Each filler type was sequentially added to vinyl-terminated PDMS at 0%, 0.5%, 5%, 10%, and 15% by weight. Tensile, tear, Durometer hardness, translucency and viscoelastic properties were evaluated, with hardness and translucency also evaluated following 3000 hours of outdoor weathering. Results demonstrated that 15% coated nano-SiO_2-filled PDMS materials produced the highest tensile strength, elastic modulus, storage modulus, loss modulus, tear strength, and durometer hardness ($p<0.05$), while 15% submicron coated SiO_2-filled materials demonstrated the highest failure strain and translucency parameter ($p<0.05$). Outdoor weathering affected hardness only for 10%- and 15%-filled submicron SiO_2 PDMS materials, but the increases were deemed too low to be clinically detectable. Only unfilled and 0.5%-filled PDMS formulations darkened from weathering, as higher filler levels offered protection against solar radiation, heat and moisture. It was concluded that superhydrophobic-coated nano-SiO_2-filled PDMS favorably produced the strongest, most tear resistant and least translucent materials, but also generated low stretch ability and high hardness that were considered to be unfavorable in achieving a “skin-like” feel.

TABLE OF CONTENTS

LIST OF FIGURES

LIST OF TABLES

LIST OF ABBREVIATIONS

a*	Red-green axis of CIE L*a*b* system
ANOVA	Analysis of variance
ASTM	The American Society for Testing and Materials
AT	Acceptability Threshold
b*	Yellow-blue axis of CIE L*a*b* system
CIE L*a*b	Comission Internationale de l'Eclairge color system
DMA	Dynamic Mechanical Analysis
DMDPS	Dimethoxydiphenylsilane
HMDS	Hexamethyldisilazane
HTV	High Temperature Vulcanizing silicone products
L*	White-black axis of CIE L*a*b* system
OEF	Operation Enduring Freedom
OIF	Operation Iraqi Freedom
PDMS	Polydimethylsiloxane
PT	Perceptibility Threshold
PVC	Polyvinyl Chloride
PVS	Polyvinyl Siloxane
RTV	Room Temperature Vulcanizing silicone products
SE	Standard Error
SEM	Scanning Electron Microscopy
TP	Translucency Parameter
UVA	Ultraviolet A
UVB	Ultraviolet B

Chapter 1: Introduction

Facial disfigurement is a distressing condition that leads to overwhelming psychological suffering, because the defects are highly visible. This causes social isolation, anxiety and depression (Lemon et al., 2005). It is often associated with an altered self-image from changes in body image, a decrease in self-esteem and a reduced quality of life (Levine et al., 2005, Nogueira et al., 2018). Facial disfigurement has been associated with unemployment, lower education level, and poor social support. A loss or impairment of critical function, such as speech and swallowing, contribute to depression, placing a person at risk for suicide (Breitbart et al., 1988, De Sousa, 2010).

Common causes of facial disfigurement include head and neck cancer, facial trauma from accident or battlefield combat, and facial burns. In 2017, head and neck cancer accounted for four percent of cancers in the United States, with an estimated 64,690 people affected (47,650 men and 17,040 women) (Head and Neck Cancer, August 2017). Seventy to ninety percent of basal cell carcinomas develop in sun-exposed head and neck regions, with five to ten percent occurring on the eyelids alone (Pratt et al., 2017). Road traffic accidents are common sources of head trauma, and internationally more than eight million people are injured, with 16.4% incurring facial injuries (Nobrega, L. M. et al., 2014). For soldiers in combat, head and neck injuries have historically constituted 16% to 21% of battlefield injuries. In current Operation Iraqi Freedom (OIF) and Operation Enduring Freedom (OEF) operations, this has increased to 29% of battlefield injuries (Owens et al., 2008). The nature of combat injuries suffered by war fighters has shifted from gunshot wounds to trauma inflicted by explosions, with explosive devices responsible for 84% of OEF/OIF craniomaxillofacial injuries (Lew et al., 2010). Modern body armor has increased survivability by reducing mortal injuries to

the chest and abdomen, but the face is left exposed (Champion et al.,2010). For facial disfigurement caused by burns, 2013 data report an incidence of 16.3 head and neck burns per 100,000 people per year in the US (Heilbronn et al., 2015).

Reconstruction of significant facial defects is still a major challenge for the reconstructive facial plastic surgeon. Surgery often involves long and complicated procedures, to which many patients are ill-suited (Thiele et al., 2015). Patients that are not willing or physically capable of receiving complete surgical reconstruction are confronted either with no treatment or prosthetic replacement. This situation makes the use of maxillofacial prosthetics critical to restoring facial disfigurement, both aesthetically and functionally (Chang et al., 2005). The prosthetic replacement has several advantages over surgical reconstruction. The process is relatively inexpensive, the fabrication process is relatively short, and unlike the surgeon, the maxillofacial clinician has complete control of the color, shape, and prosthesis position. Disadvantages include possible irritation of the tissue site, fungal infection on the intaglio surface, the need for periodic remakes, and reliance on adhesives or some other form of retention (Lemon et al., 2005).

Aesthetics is an essential factor in the acceptance of a facial prosthesis. The ideal material should look and feel like normal facial tissue and maintain these properties during the lifetime of the prosthesis (Eleni et al., 2009). It should exhibit high toughness, tear strength, tensile strength, and elongation at break, with surface hardness resembling that of the patient's skin (Hatamleh & Watts, 2010). A patient's perception of the outcome and satisfaction with treatment are critical elements in evaluating the quality of care, but are often absent in clinical studies (Chang et al., 2005). Unfortunately, it is reported that 12% of patients who receive an ear, nose, eye, and cheek prosthesis never wear them (Chen et al., 1981). It has been reported that 15% of patients do not wear their prostheses because they do not like the appearance of the device. Acceptance of a

prosthesis also is related to the psychological nature of the patient (Jani & Schaaf, 1978). Prosthesis longevity is a major problem, and it has been reported that the wearing time is approximately 6–12 months (Stathi et al., 2010). Another study reported the lifetime to range between six and 24 months, at which time physical and mechanical property deterioration, discoloration, and delamination of the retentive substrate is observed (Hatamleh et al., 2016). Clinical experience has indicated the need for frequent replacement of facial prostheses (Haug et al., 1999).

The most widely used materials for maxillofacial prostheses are silicone elastomers (Lai et al., 2002). Silicones are chosen because of their chemical inertness, satisfactory strength, durability, ease of manipulation, and biocompatibility (Aziz et al., 2003b). Silicone has been proposed as the best material to rehabilitate patients with craniofacial defects (Brandao et al., 2017) because its flexibility delivers better comfort to the patient (Nobrega et al., 2016).

Filled polydimethylsiloxane (PDMS), a silicone, is the most common material used in the construction of facial prostheses (Polyzois et al., 2011). The quality of these materials depends greatly on their two primary components, the PDMS polymer and the silica fillers. These components and their interactions affect the overall strength, service lifetime and biomimetic texture of the prosthesis (Aziz et al., 2003b; Bellamy et al., 2003). However, the surface texture is a commonly reported problem, along with discoloration, lack of longevity, material degradation, margin deterioration, and decreased mechanical adequacy. The current generation of maxillofacial prosthetic materials is perceived as too stiff and not mimicking the natural feel of skin (Tetteh et al., 2017)

Research is ongoing to develop new polymeric materials with superior mechanical properties and are more “skin-like” in their feel. Recent research has focused on incorporating nanoparticle fillers into the organic polymer matrix, creating a

nanocomposite that better combines the strength of the filler with flexibility of the organic matrix (Goiato et al., 2010). Previous research reported that the addition of 5% by weight nano-SiO_2 to polydimethylsiloxane produced elastomers with good stretchability and strength while maintaining low stiffness. These conditions were deemed essential to achieving a proper texture and “feel” in a maxillofacial prosthesis (Duevel et al., 2015). Other research reported increases in tensile strength, tear strength, and percentage elongation when 3% by weight nano-SiO_2 is added to commercial PDMS materials containing conventional submicron size fillers. This is expected to permit construction of a prosthesis with a thinner margin that offers greater stretching and a lower chance of tearing (Zayed et al., 2014)

Evenly dispersed nanoparticles is key to achieving uniform material properties. Therefore, recent attention has been given to a class of hydrophobic coatings that are sometimes classified as “superhydrophobic.” The coatings are expected to invoke repulsion among particles and thereby assist in separating nanoparticles during their incorporation into polymer. In principle this should produce a more uniformly distributed filler phase. The purpose of this thesis research project is to study PDMS filled with uncoated and hydrophobic-coated nano-silica (nano-SiO_2) and compare their mechanical behaviours with those measured for a conventional submicron-filled PDMS.

Given this background information, we hypothesize that sequential additions of superhydrophobic-coated nano-SiO_2 to PDMS will generate improved physical properties than observed with PDMS filled with either uncoated nano-SiO_2 or conventional submicron-filled silica.

Chapter 2: Literature Review

2.1 Historical Development and Requirements for Maxillofacial Prosthetic Materials

Throughout history, materials used to replace missing parts of the maxillofacial region include wood, ivory, waxes, and metals (Andres et al., 1992). Later materials introduced for maxillofacial prostheses include latex, poly (methyl-methacrylate), vinyl chloride polymers, polyurethane, acrylic resin, and silicone (Chalian et al., 1974). Since 1960, silicon-based elastomers have been used to fabricate maxillofacial prostheses due to their flexible mechanical properties and translucent optical properties (Barnhart, 1960). Attempts at reproducing color characteristics of human skin by prosthetic materials have been measured using color analysis by reflectance spectrophotometry (Cantor et al., 1969).

The criteria for ideal maxillofacial materials are that they should not irritate the surrounding tissues yet permit sufficient strength at the periphery of the prosthesis to prevent tearing, particularly when an adhesive has been placed. The materials should provide translucency, color matching with skin, low weight, easy processing, and easy manipulation prior to processing (Chalian & Phillips, 1974). Sweeney et al. (1972) evaluated polyvinyl chloride (PVC) and established key properties required when formulating new maxillofacial prosthetic materials, which are used to this day. These properties include: (1) ease of molding, as each case necessitates an individual mold (2) an ability to allow colors and shades to mimic the patient's skin characteristics, (3) flexibility, to approximate the mechanical properties of natural tissues, (4) chemical stability under average conditions, (5) tear and abrasion resistance when shaped to a very thin edge, (6) color persistence against radiation (sunlight),skin oils and fluids

exposures for prolonged periods of time, and (7) ease of replication or substitution by technically qualified, non-professional personnel. Physical properties identified and tested were tensile properties, hardness, stiffness, tear resistance and thermal stability (Sweeney et al., 1972).

As flexibility was considered as one of the important properties for maxillofacial materials, Koran and Craig (1975) evaluated the dynamic physical properties of PVC, polyurethane, and PDMS using a Goodyear Vibrotester. This study found that PDMS possessed the most stable dynamic properties and provided a distinct advantage for service as a maxillofacial material (Koran et al., 1975). Craig et al. (1978) evaluated the color stability of PVC, polyurethane, and silicon elastomer after accelerated aging, using reflectance spectrophotometry. All materials were placed for 900 hours in a Weather-Ometer and evaluated by determining luminous reflectance, contrast ratio, dominant wavelength, and excitation purity. It was concluded that silicone elastomers demonstrated good color stability and were the most promising materials for maxillofacial prostheses (Craig et al., 1978). Based on these studies, results suggested PDMS as the optimum maxillofacial prosthetic material.

2.2 Fundamental Composition and Setting Reactions of Polydimethyl Siloxane

PDMS currently is the most commonly used elastomer for a maxillofacial prosthesis. Polymerization of PDMS is achieved through chemical linking of polymer chains, and incorporation of silica fillers that improves the physical and mechanical properties of the material. Through a cross-linking reaction, siloxane polymers can be easily transformed into a three-dimensional network which allows the formation of chemical bonds between adjacent chains, (Coles et al., 2004). PDMS has molecular weight ranging from 9000 to 50,000 (Meyers et al., 1980).

Three primary polymerization modes are employed for PDMS used as facial materials. Polymerization of base elastomers that constitute the bulk of a prosthesis is achieved through condensation or addition crosslinking reactions. For condensation, when cured at room temperature, PDMS terminated with hydroxyl groups undergoes polycondensation in the presence of a tin catalyst, and the resulting material is known as room temperature vulcanizing (RTV) silicone. The second mode is a heat-cured system in which unsaturated vinyl- terminated polysiloxanes undergo free radical addition with the aid of a platinum catalyst and polymerize at elevated temperatures (approximately 85°C to 100°C). These elastomers are known as high temperature vulcanizing (HTV) elastomers (Figure 5.1, Aziz et al., 2003a; Colas et al., 2004). HTV elastomer is the most commonly used material in facial prosthesis fabrication. Acetoxy polymerization is the third mode and is used to paint pigments on the surface of the prosthesis, which is mixed and polymerized in open air. The acetoxy cure system is a tin-catalyzed moisture-cure system which generates an acetic acid by-product upon curing. (White et al., 2010).

The strength of silicone polymers without filler is generally unsatisfactory for most applications. The addition of reinforcing fillers reduces silicone's stickiness, increases its hardness and enhances its mechanical strength. Generally, the most favorable reinforcement is obtained using silica (Colas et al., 2004). Reinforcement occurs with polymer adsorption encouraged by the silica's large surface area and when hydroxyl groups on the surface of filler lead to hydrogen bond formation with the silicone polymer. This produces silicone rubbers with high tensile strength and elongation capability (Lynch, 1978). Chemical treatment of the silica filler with silanes further improves silicon elastomer's incorporation and reinforcement, resulting in increased material strength and tear resistance (Colas et al., 2004). Incorporation of a hydrophobic surface-treated silica filler with a low particle size creates a high surface area for polymer adsorption and

permits better dispersion into the uncured silicone polymer than do non-surface-treated filler systems (Aziz et al., 2003b).

2.3 Esthetic Properties

The ideal maxillofacial prosthesis must achieve color, texture, form and translucence that duplicate missing structures and adjacent skin (Mahajan et al., 2012). In the manufacturing process, silicone elastomers are colored with a variety of pigments to establish a good color match between elastomer and natural skin. There are two general methods for coloring maxillofacial elastomers, which involve intrinsic and extrinsic coloring. Intrinsic coloring involves the incorporation of internal color within the base elastomer. Extrinsic coloring is the process that brings a facial prosthesis 'to life' by adding surface details such as freckles, veins, hair or natural areas of shadow (Thomas, 1994). Coloration is accomplished by using oil-based, dry rare-earth, glass or ceramic pigments. The pigments are incorporated into the elastomer before polymerization to achieve a baseline color, and final customization is improved by painting a thin layer of pigmented siloxane adhesive onto the surface of a prosthesis (Beatty et al., 1999).

One of the most critical properties of maxillofacial prostheses is color stability, and substantial research has been conducted to study this problem. Craig et al. (1978) reported one of the first attempts to test the color stability of facial elastomers using an artificial weathering approach. In this study, color stabilities of polyvinyl chloride, polyurethane and silicone elastomers for maxillofacial applications were determined after accelerated aging using reflectance spectrophotometry. This study found silicone materials were the most promising materials in terms of color stability after accelerated aging and for ease of processing (Craig et al., 1978). Later, Koran et al. (1979) investigated color stability of a series of dry mineral earth maxillofacial pigments on

silicone elastomers. This study determined the color stability after accelerated aging using spectrophotometry and concluded that seven of the pigments (dark buff, medium brown, light brown, red brown, black, red, and blue) demonstrated good to excellent color stability, while four pigments (white, light orange, yellow, and orange yellow) were less promising for clinical usage (Koran et al., 1979).

Beatty et al. (1995) researched the color changes in A-2186 elastomer with dry rare-earth pigments, uncolored and colored, after exposure to ultraviolet-A and ultraviolet-B lighting. They found that unpigmented elastomer underwent color changes after storage darkness for 45 days, and cosmetic red and cadmium yellow pigments underwent significant color change after 400 hours of UVA and UVB light exposure. Santos et al. (2010) studied color stability of colorless and pigmented silicone elastomers after accelerated aging using spectrophotometry. They combined organic and inorganic pigments for the pigmented elastomer. In this study, they found that non-pigmented materials presented the lowest values of color alteration compared to the pigmented materials. It was concluded that the pigment's incorporation appeared to be the main cause of color instability of silicone (Dos Santos et al., 2010).

A significant clinicians face in prosthetic rehabilitation is to achieve a good balance when color matching facial prostheses with the surrounding skin. Paravina et al. (2009) stated that color difference tolerances can be determined by asking two questions, "Can I see a difference in color?," for a perceptibility judgement, and "Is this difference in color acceptable?," for acceptability judgements of color differences. It has been stated in dentistry that a nearly perfect color match corresponds with a color difference below the 50:50% perceptibility threshold (PT), which refers to a color difference that can be detected by 50% of observers, while the other 50% observers cannot see any difference. Accordingly, an acceptable color match represents a

difference in color below the 50:50% acceptability threshold (AT), where the color difference is described as acceptable by 50% of observers (Paravina et al., 2009).

Matching both color and translucency characteristics of a prosthesis with those of human skin is highly important for a successful appearance match. Even when the shape and texture of the prosthesis do not perfectly duplicate human skin, the prosthesis will be less noticeable if the coloration and translucency match under different lighting conditions (Andres et al., 2000). Translucency can be quantitatively described using a translucency specification such as transmittance, contrast ratio and translucency parameter, each of which involve optical measurements performed at a specified thickness. The translucency parameter (TP) was developed to relate human visual perception to the translucency of a pigmented material. TP is measured as the color difference between the reflected colors of a material with defined thickness positioned over black and white backings (Hu et al., 2011).

The TP ranges from 0 as completely opaque to 100 as perfectly translucent. To match the color and translucency of maxillofacial prosthesis with a patient's skin involves adding pigments to first establish a close translucency, then adding additional pigments to obtain a suitable color match (Johnston et al., 1995). A certain amount of translucency is needed to permit adequate coloration; however, opacity also is essential to block out colors from underlying facial structures. No desired TP values have been published thus far for maxillofacial elastomers.

2.4 Physical Properties

A facial prosthetic material should have sufficient flexibility to provide comfort when in contact with movable tissue, possess high tensile strength, high percent elongation, skin- like elastic modulus, high tear strength, dimensional stability, low weight, good edge strength, and low thermal conductivity. Essential physical properties

used for the construction of maxillofacial prostheses are described in the following sections.

2.4.1 Tensile Properties

Tensile strength of the silicone elastomer indicates overall strength of the material and the elongation under load reflects prosthesis stiffness. These properties provide information on the materials' abilities to deform under mechanical stress. High tensile strength and elongation are desired, especially when the feathered edges of the prosthesis are peeled away from the facial tissue. (Aziz et al., 2003b; Bellamy et al., 2003).

By measuring the material while it is being pulled, tensile properties can be obtained. When plotted on a graph, these data produce a stress/strain curve, which permits identification of strength, elastic modulus and strain. Ultimate tensile strength is the maximum stress that a material can withstand. Elastic modulus is a measure of the material's stiffness, which measures the resistance to elastic deformation. Strain is the amount of stretch or elongation that a material undergoes in response to stress. Therefore, it is important to measure tensile properties to gain information regarding strength, stiffness and stretchability during prosthesis usage. Classic work by Lewis and Castleberry (1980) established values for tensile strength and elastic modulus to be 1000-2000 psi (6.89-13.78 MPa) and 50-250 psi (0.34-1.72 MPa), respectively.

2.4.2 Tear Properties

The tear strength of a maxillofacial material is extremely important, particularly at the thin margins surrounding nasal and orbital prostheses. A thin margin helps mask the presence of a facial prosthesis where it blends into the surrounding facial tissue. When the facial prosthesis is removed, the thin margins are susceptible to tearing as the

prosthesis is peeled away from facial tissues. (Aziz et al., 2003b). Margins are usually glued with medical adhesive and are highly susceptible to tearing when the facial prosthesis is removed at nighttime for cleaning (Hatamleh et al., 2010). Thin and fine prosthesis margins require greater tear strength in order to blend them with skin surrounding defect site, and endure repeated removal (Bellamy et al., 2003; Nobrega et al., 2016). Optimization of tear strength can be accomplished by incorporating low molecular weight polymers into the base elastomer, which introduces a broader distribution of high cross-link density networks. However, this might tighten and produce brittle networks with limited flexibility (Aziz et al., 2003b). Based on Lewis and Castleberry's results (1980), a desired value for tear strength is 30 - 100 ppi or 5.25 – 17.51 N/mm.

2.4.3 Viscoelastic properties

Viscoelasticity is the property of materials that exhibit both viscous and elastic characteristics when undergoing deformation. An ideal maxillofacial prosthetic material should have viscoelastic properties comparable to those of facial and oral tissues to be replaced. When loaded and unloaded, viscoelastic materials undergo both immediate and time-dependent deformation responses. A common test for measuring viscoelasticity is Dynamic Mechanical Analysis (DMA), where a sinusoidal force is applied and the corresponding deformation is measured. Immediate deformation, or that which accompanies the applied force, is elastic in nature and the corresponding stiffness is recorded as the storage modulus. Time-dependent deformation occurs when an amount of lag time occurs between the applied force and the deformation response. This reflects material damping and is measured by the loss modulus. A third parameter, tan delta, is the ratio of the loss modulus to the storage modulus and provides an indicator of the relative amount of viscous deformation occurring with respect to corresponding

storage modulus at any point in time. A spike in tan delta often indicates transitions occurring within the molecular structure of a polymer at a given temperature or time point. This helps identify key parameters such as glass transition temperature (Tg) and crystallization temperature (Gupta et al., 2009). Because texture and feel play a role in viscoelasticity, the dynamic mechanical properties of silicone elastomers can greatly affect the clinical success of maxillofacial applications (Murata et al., 2003).

Koran and Craig (1975) evaluated dynamic physical properties of PVC, polyurethane, and PDMS using a Goodyear Vibrotester. This study found that PDMS possessed the most stable dynamic modulus over the temperature range of -15 to 37^{o}C, while PVC's and polyurethane's dynamic moduli were affected by those temperature ranges. The rapid increase in dynamic modulus with decreasing temperature for PVC was considered to be a drawback for its use in temperate climates. Therefore, the stability from PDMS was considered to offer a distinct advantage for service as a maxillofacial material (Koran et al., 1975).

Mouzakis et al. (2010) investigated the dynamic mechanical properties of silicone when incorporating several concentrations of zinc oxide (ZnO) additives. They found that there was no influence of ZnO additives on storage and loss moduli. Viscoelastic properties of medical grade silicone were studied by Mahomed et al. (2008). Because elastomers are viscoelastic, loading frequency is expected to alter silicone behavior. They found that storage modulus, loss modulus, and tan delta depended on loading frequency; since the silicone elastomers undergo a transition from the rubbery to the glassy state above 0.3 Hz (Mahomed et al., 2008). Chiulan et al. (2020) evaluated the viscoelastic behavior of unfilled silicone and silica-filled silicone using DMA. They observed a significant lowering of storage modulus with increasing temperature in all samples, especially for unfilled silicone. Presence of silica fillers acted to reduce the negative impact of cyclic stress (Chiulan et al., 2020).

2.4.4 Surface Hardness

Hardness of a maxillofacial silicone elastomer is a measure of material compressibility, and it is desirable to have a material with softness similar to adjacent facial tissues. The texture should be close to that of human skin, otherwise, the facial prostheses will seem lifeless, despite perfect sculpture and adaptation (Goiato et al., 2009). Hardness of the maxillofacial silicone elastomer also reflects its flexibility, and it is desirable to have a material with similar softness to facial tissues surrounding the defect site (Bellamy et al., 2003).

With compositional differences, silicone elastomers exhibit a wide range of Shore A hardness values. Lewis and Castleberry (1980) recommend the values to range between 25 to 35 Shore A units, which are representative of skin tissue, depending upon the facial region being restored (Bellamy et al., 2003). Hardness increases are often achieved by increasing filler content, which provides better reinforcement and higher stiffness. Material usage also may affect hardness, and for facial elastomers, exposure to ultraviolet radiation degrades the polymers through radiolysis. This mechanism enhances cross-linking and produces smaller molecular weight chains with shorter distance between crosslinks. This increases hardness (Hatamleh et al., 2010; Cottin et al., 2000; Eleni et al., 2011).

2.5 Degradation of Polydimethyl Siloxane

Maxillofacial prosthetic materials ideally should be stable over time, and durable for at least 6 months without compromising esthetic and physical properties. Material challenges experienced during prosthesis wear include exposure to ultraviolet radiation, oxygen, adherent materials, temperature change and fluids such as water or sebum. Prosthesis deterioration is manifested as a degradation of physical, static and dynamical

mechanical properties, and gradual discoloration in a service environment (Polyzois, 1999). Prosthesis handling, wear and exposure to the surrounding environment underlie the observed material changes. As a prosthesis must be removed and cleaned daily, the material is subjected to adhesive-removing solvents, surface rubbing, and water exposure during washing. During daily wear, its surfaces contact bodily fluids such as saliva, perspiration and tissue fluids, which may continually seep onto the intaglio surface. Environmental factors, such as exposure to ultraviolet (UV) radiation, temperature change, abrasion from contact with dust particles and humidity contribute to prosthesis deterioration (Nguyen et al., 2013, Tetteh et al., 2017).

Silicones degrade upon exposure to UV radiation at wavelengths of 300 nm and above (Wypych, 2008). UV radiation, which enhances cross-linking and increases breakdown of the polymer, ultimately decomposes the elastomer (Hatamleh et al., 2010). Ultraviolet radiation liberates protons, and in the presence of oxygen contributes to photo-oxidative degradation. Energy photons or particles (gamma rays, protons, electrons), with energy greater than the strength of the molecular bond, degrade the polymer through radiolysis, and generate free radicals (Cottin et al., 2000). This invokes competition among initiation, propagation, and termination steps in the addition polymerization process. Ultimately this leads to polymer molecule degradation with the production of smaller polymer chains and volatile oligomer degradation products. This polymerization disturbance causes changes in the molecular weight distribution, which negatively affects the physical and chemical properties of the material (Eleni et al., 2011).

2.6 Manufacturing and Handling Properties

The raw materials of an ideal prosthetic material must be easily produced and inexpensively fabricated. The material should be a castable solvent-free liquid having an appropriate viscosity and working time. Absence of solvents is necessary to avoid bubbles and to minimize shrinkage; ideally no shrinkage should occur. The viscosity should be low enough to allow the liquid to enter the most complex parts of a mold and faithfully replicate the mold surface (Lewis et al., 1980). Working time prior to polymerization should be sufficient, polymerization should occur at low enough temperatures to permit reusability of molds, and the material should be adaptable to intrinsic and extrinsic coloration (Mahajan et al., 2012).

Traditional prosthesis production is a long and labor-intensive process, requiring the use of several invasive and subjective techniques during fabrication. Typically, the process begins with an alginate impression of the defect area and formation of a plaster cast to establish a template for the prosthesis. A wax replica of the missing tissue is constructed directly on the cast, inserts such as magnets are placed, and plaster is poured on top of the wax-reconstructed model. Once the second plaster cast has set, the two casts are separated, the wax boiled away and pigmented elastomer placed into the space once occupied by the wax. The two casts are pressed together and heated to polymerize the elastomer. The process potentially creates mistakes (Mohammed et al. 2016).

Considering the lengthy process for prosthesis construction, intense effort is currently devoted to developing 3D printing technologies that will reduce the amount of time and materials needed, and permit layering with different pigments that should provide a more life-like depth of color in appearance. Modern optical scanning techniques allow for rapid and high-resolution reproduction of surface topography with precision of <100 μm and could procure useful data such as texture maps of a patient’s

skin (Palousek et al. 2013). Scanned images will remove the need for invasive procedures and Computer Aided Design software will permit design iterations to be stored indefinitely without the need for a physical model. (Mohammed et al., 2016).

2.7 Nanoparticles

A nanoparticle is defined as a particle of matter with sizes between 1 and 100 nanometers (nm) in diameter. Nanoparticles can be spherical, cubic or needle-like (Cushing et al., 2004). As a particle is reduced in size from micrometer to nanometer, the resultant properties can change dramatically (Allaker et al., 2008). Matrix voids adjacent to large-sized particles can serve as pre-existing cracks. These large particles diminish load transfer to a soft matrix, which reduces material reinforcement and lead to degraded mechanical properties (El-Kady et al., 2014). This suggests that reducing particle size is key to improving the strength of composite materials. Smaller particles have a higher total surface area for a given particle loading. This indicates that strength increases with increasing particle surface area through a more efficient stress transfer mechanism (Fu et al., 2008). However, adding high filler content to polymer matrix with smaller particles dramatically increases viscosity, which worsens handling properties.

Nanoparticles are widely incorporated into industrial materials such as textiles, rubbers, sealants, plastics, cosmetics, fibers, coatings, sunscreens, dental composites and toothpastes. In dentistry, nanoparticles are added to dental composites to improve the tooth-composite interface continuity and adhesive strength. Nanoparticles are playing an increasing role, as they are intentionally embedded into products to improve material properties. Examples are improved polishability and gloss stability in resin-based composites and as components for tissue engineering scaffolds. Examples are the use of nano-hydroxyapatite to fill hydrogels for placement into bone healing sites (Schmalz et al., 2017; Chieruzzi et al., 2016), and improved dentifrices that better reduce

plaque formation and whiten teeth (Tang et al., 2006). In elastomers, enhanced mechanical properties through nanoparticle additions may be attributed to a higher surface energy and chemical reactivity, which allow the nanoparticles to interact with the siloxane backbone and form a three-dimensional network (Watson et al., 2004).

Silicon dioxide nanoparticles (SiO_2), or silica, have increasingly been used for numerous biomedical and biotechnological applications. Drug molecules are loaded into silica nanoparticles. Silica's biocompatibility makes it a benign material (Schooneveld et al., 2008). SiO_2 nanoparticles are characterized by their small size, large interface area, active function, and strong interfacial interaction with an organic polymer. Therefore, they can improve the physical, mechanical, and optical properties of the polymer and provide resistance to environmental stress-induced cracking and aging (Han et al., 2008). SiO_2 is used widely as a filler material in the submicrometer size range to improve the mechanical properties of siloxane elastomers. SiO_2 exists in many crystalline forms (polymorphic), but in most cases tetrahedral SiO_4^{4-} units are linked together with shared vertices in various arrangements. Silica nanoparticles have been used in paints to control rheological properties and serve as reinforcing fillers in nanocomposites in order to improve tensile strength and wear and scratch resistance (Zheng at al., 2003).

It is imperative to maintain nanofiller content at a proper level because of their higher surface energy and chemical reactivity, otherwise, the nanoparticles may agglomerate. When the silicone elastomer is under external forces, agglomerated particles act as stress concentrating centers within the elastomer matrix, thereby decreasing mechanical strength (Han et al., 2008). Efforts have been devoted to preventing agglomeration of nanosilica by coating silane coupling agents onto particle surfaces. Depending upon the type of coupling agent, the inorganic filler particle can be attracted and/or chemically bound to the organic matrix. (Zayed et al., 2014). Surface-treated silica fillers are also better at dispersion into the silicone elastomer and have a

reduced base viscosity, compared to non-surface-treated fillers. Under deformation, these fillers increase elastomer strength by allowing the polymer chains to uncoil and slide past neighboring filler particles, thereby promoting crystallization between neighboring PDMS chains (Santawisuk et al., 2010).

Recently, “superhydrophobic” coatings have been adsorbed onto nanosilica surfaces as a means to improve dispersion and interaction with polymer molecules. Superhydrophobic surfaces exhibit extremely high-water repellency, where drops of water bead up on the surface, roll with a slight applied force, and bounce if dropped onto the surface from a height (Xie et al., 2018). Typically, a surface is termed superhydrophobic when the water contact angle exceeds 120^{o} or 150^{o} (Arkles, 2006; Chang et al., 2009).

To date, limited research has been conducted to evaluate physical property effects rendered by nanoparticle additions to PDMS prosthetic elastomers. Han et al. investigated the mechanical properties of submicron-containing commercially available elastomers with the addition of various concentrations (0.5%, 1.0%, 1.5%, 2.0%, 2.5%, or 3% by weight) of nanosized oxides (Ti, Zn, or Ce). They found that the 2.5 weight percent additions produced 5 times higher tensile strength and 2 times higher tear strength. However, 3.0% nano-oxides were observed to be partly agglomerated within the silicone specimens, which caused tensile strength to be 3 times lower and tear strength to be 1.6 times lower (Han et al., 2008).

Cevik et al. (2017), studied the addition of 10 volume percent titanium dioxide (TiO_2), fumed hydrophilic SiO_2, and silane coated hydrophobic SiO_2 nanoparticles in two different RTV silicone elastomers, and investigated their effects on mechanical properties. The silane-coated hydrophobic SiO_2- filled materials demonstrated significantly higher tensile strength (2.3 and 1.2 times higher respectively) and higher percent elongation (2 and 1.2 times higher respectively) compared toTiO_2- filled

materials and fumed hydrophilic SiO_2. Because this study did not report dispersability of the different nanoparticles, the underlying reasons for these differences were unclear. Research involving other polymer systems have yielded confusing information regarding the amount of filler allowable for adequate dispersion into polymer. One study reported that for a polymethyl-methacrylate system, no more than 0.9% by volume nano-SiO_2 could be dispersed (Balos et al., 2014), whereas other findings showed successful dispersion up to 50% by weight concentration of nano-SiO_2 in polyurethane (Petrovic et al., 2000). Collectively, published reports on nanoparticle incorporation into polymer systems intended for prosthetic applications furnish limited guidance for engineering improved materials.

2.8 Gap in Knowledge

To date, limited research has been conducted to understand the role that nanoparticle addition renders on PDMS elastomers intended for maxillofacial applications. Existing data are based upon research that fails to control for polymer chemistries, filler loadings, particle sizes and filler surface treatments. The purpose for this research is to study physical property changes occurring in nano-silica-filled PDMS elastomers where filler size, loading and surface treatment are controlled. This study will focus on the effects of filler content and presence/absence of hydrophobic surface coating, where filler size and polymer chemistry are held constant. Results will be compared to “conventional” PDMS materials loaded with a standard submicron-sized particle.

Chapter 3: Materials and Methods

3.1 Preparation of Samples

Elastomers were constructed by combining vinyl terminated PDMS, SiO_2 fillers, crosslinker and platinum catalyst, then polymerizing the mixture under heat. Three types of SiO_2 fillers, 15 nm coated nano-SiO_2 (KH220), 15 nm uncoated nano-SiO_2 and 200 nm submicron SiO_2 (TS530) were used for this project. Nano-SiO_2 were chosen based on previous research at UNMC that the addition of 5% nano-SiO_2 to PDMS produced high strength elastomer and good ability to stretch while maintaining low stiffness. Submicron SiO_2 was chosen as a control because it is a conventional filler in PDMS. The materials used are presented in Table 3.1.

Table 3.1 Materials and Manufacturers

Materials	Manufacturers
V2K Vinyl-Terminated PDMS	Momentive Materials, Tarrytown, NY
15 nm Dimethoxydiphenylsilane-coated nano-SiO_2 (KH220)	US Research Nanomaterials, Inc. Houston, TX
15 nm Uncoated nano- SiO_2	US Research Nanomaterials, Inc. Houston, TX
200 nm Hexamethyldisilazane-coated SiO_2 (TS530)	Cabot Corporation, Boston, MA
V-XL crosslinker	Momentive Materials, Tarrytown, NY
10 ppm Platinum catalyst	Momentive Materials, Tarrytown, NY

For elastomer preparation, each type of filler was sequentially added to vinyl terminated PDMS at 0%, 0.5%, 5%, 10%, and 15% by weight. The filler particles were first incorporated using a rotary mixer (ME 100L, Charles Ross and Son Company, Hauppauge, NY) at 5000 rpm for ten minutes. For nanoparticles (KH220 and Uncoated), an ultrasonic processor (Hielscher model UP200S, Teltow, Germany) was applied for ten minutes at 105 W/cm^2 to burst nanoparticle agglomerates. Each mixture was contained in a 100 ml stainless-steel cup that was cooled in an ice bath over a ten-minute period. After removal from the ultrasonic mixer, the mixture was rotary mixed again with a Cowles disperser for ten minutes at 5000 rpm to achieve a uniform distribution of nanoparticles. For traditional submicron particles (TS530), rotary dispersion was accomplished without ultrasonic treatment, following mixing protocols normally followed for conventional silicone elastomer.

For polymerization, the filler-containing vinyl-terminated PDMS was combined in a 1: 1 molar ratio with polymethyl hydrogen siloxane (V-XL crosslinker) and 10 ppm platinum catalyst. The mixtures were hand-mixed in a paper cup using a wooden tongue depressor for about two minutes, then placed into a high vacuum pump (8920 Vacuum Pump DirecTorr, Welch Vacuum Technology, Skokie, IL) under 5 x 10^{-3} torr constant vacuum. Bubble removal was visually checked, usually requiring five to ten minutes. The bubble-free mixture then was slowly poured into a mold, and a lid was placed with sufficient pressure to squeeze out excess material. The pressed mold was placed into an 85^{o}C oven for sixty minutes for polymerization.

Two types of molds were used in this project. For tensile properties, elastomer mixtures were poured onto a rectangular gypsum mold, covered and tightened with six clamps to extrude excess materials. This mold produced 245 mm length x 165 mm width x 2 mm thickness elastomer sheets. Dumbbell-shaped samples were cut from elastomer sheets using ASTM D412 die C die cutter to produce twelve samples for each group

(ASTM International, 2002). Twelve samples per group was chosen from this test based on the previous conducted tests by Willet et al. that showed ten or more samples produced significant differences (Willet et al., 2015). For tear strength, the same mold was used to make the elastomer sheets and ASTM D624 die C die cutter was used to construct ten samples (ASTM International, 2001). Ten samples per group was chosen from this test based on the previous conducted tests (Willet et al., 2015) that showed ten samples gained significant differences.

For durometer hardness and translucency parameter, molds were assembled from polyvinyl chloride (PVC) pipes cut into 6 mm thick rings. Each ring was placed onto a gypsum block and held in place by injecting medium-body polyvinyl siloxane (PVS) impression material around the periphery. The siloxane mixture then was poured slowly into the mold and a glass lab placed on top to squeeze out excess material. This mold created a 33 mm diameter x 6 mm thickness disc, as compliant with ASTM D2240 (ASTM International, 2005). Each of the filler loading groups in three different types of filler were divided into two subgroups, one for indoor storage and the other exposed to outdoor weathering with five discs per subgroup. Five samples were chosen based on the previous conducted tests (Willet et al., 2015) that showed five samples gained significant differences for durometer hardness.

3.2 Physical Properties Measurements

3.2.1 Tensile properties measurements

A universal testing machine (Instron 1123-5500R, Instron Corp., Boston, MA) controlled by Bluehill 3 software were used to perform tensile testing and record tensile strength, elastic modulus and failure strain data. ASTM D412 die C sample shape and dimension can be seen in Fig. 3.1, and the testing protocol followed the tensile test procedure described in ASTM D412 (ASTM International, 2002). The sample was

loaded into pneumatic grips with 30 psi pressure and a gauge length of 25 millimeters. The dumbbell was elongated at 500 mm/min rate while the computer recorded stress versus strain data until failure.

Force and elongation measurements were recorded electronically and the resulting stress–strain tensile curves were constructed according to these equations (Eleni et al., 2009):

$$\sigma = \frac{F}{A} \qquad \varepsilon = \frac{\Delta L}{L_0}$$

where σ is stress and ε is strain. F and ΔL, are the force and deformation respectively, which were recorded electronically, while A is the cross-section area and L_0 is the initial length of the samples.

Three properties measured were ultimate tensile strength, total strain at failure, and elastic modulus. These properties were chosen to determine strength, stretchability and stiffness of the prostheses. Ultimate tensile strength was considered to be the maximum stress (MPa) the material could withstand. Failure strain was the total amount of material extension before failure, calculated by maximum displacement divided by the original (standard) length (mm/mm). Elastic modulus was the material's resistance to elastic deformation and calculated as the slope of the linear portion of the stress-strain curve.

3.2.2 Tear Strength Measurement

The same universal testing machine and software used for tensile properties also performed tear strength measurements. ASTM D624 die C sample shape and dimension can be seen in Fig. 3.2, and the testing protocol followed the tensile test procedure on ASTM D624 (ASTM International, 2001). The un-nicked test piece was measured for

thickness and width then loaded into pneumatic grips with 30 psi pressure. The rate of jaw separation was 500 mm/min and the maximum force was recorded until rupture.

Tear strength is defined as the maximum force required to break the sample divided by its thickness and calculated using the following equation (Bellamy et al., 2003):

$$T_s = \frac{F}{t}$$

where T_s is the tear strength (N/mm), F the load at failure (N), t the thickness of specimen (mm).

3.2.3 Shore A Hardness Measurement

The previously described sample discs were used for durometer hardness (n=10 per group). Each of the filler loading groups in three different types of filler were divided into two subgroups, one for indoor storage (n=5) and the other exposed to outdoor weathering (n=5). Indoor samples were placed inside a closed box held within a controlled temperature and humidity darkroom at the Biomaterials Laboratory, College of Dentistry, University of Nebraska Medical Center. Outdoor samples were placed on the roof of Keim Hall located at the East Campus University of Nebraska-Lincoln. The samples were placed on racks as seen in Fig. 3.3. Weathering was performed for 3000 hours which represent approximately 3 years of prothesis clinical year (approximately three hours of sun exposures per day). Weathering exposures commenced July 1, 2019 and ended November 5, 2019. After 3000 hours, the samples from all groups were retrieved, the disc surfaces rinsed with distilled water to remove dust, and then air-dried for about 5 minutes. Hardness measurements were taken before and after weathering with a shore A hardness tester mounted on a loading stand. Following protocols specified in the ASTM D2240 standard, five measurements were taken at five different

points on a disc's surface, and the average of five readings were determined to be a hardness value for one disc.

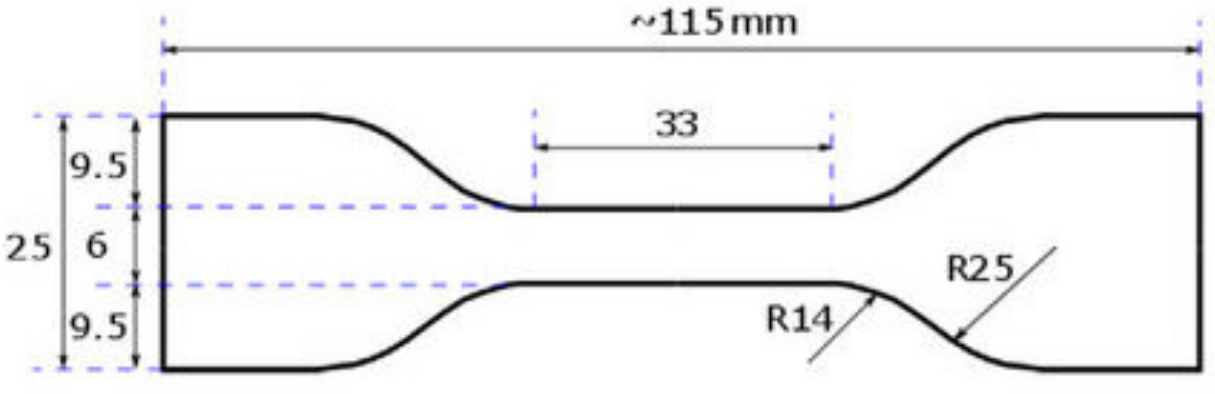

Figure 3.1 ASTM D412 die C sample dimension for tensile properties measurements

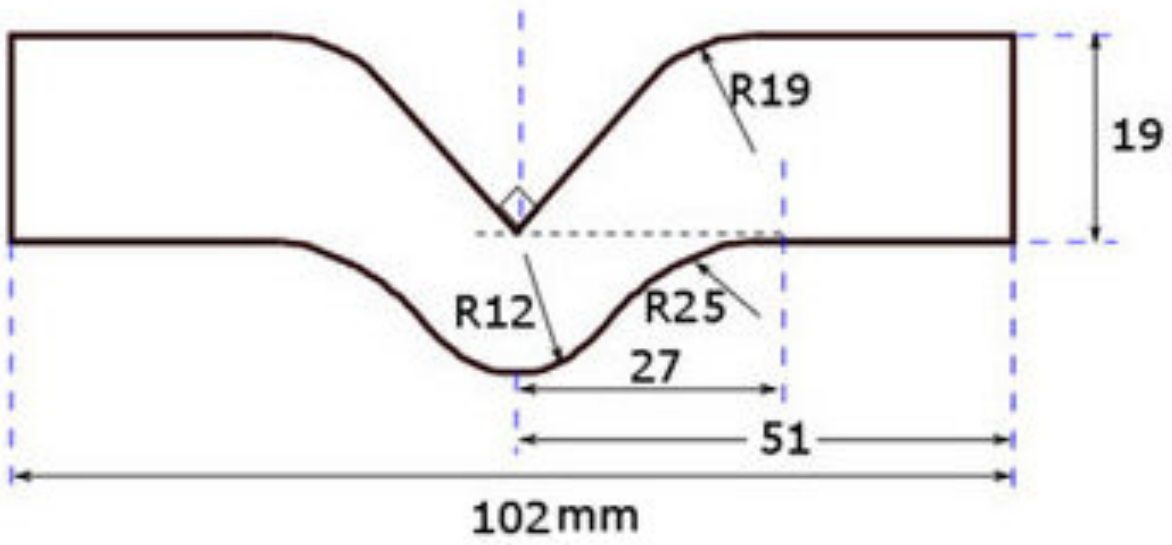

Figure 3.2 ASTM D624 die C sample dimension for tear strength measurement

Figure 3.3 Discs on the weathering rack for outdoor weathering

3.2.4 Translucency Parameter Measurement

Discs constructed for the Durometer hardness test also were used to measure translucency changes before and after weathering. A color reflectance spectrophotometer (CM-2002, Konica Minolta Corp., Ramsey, NJ) with computer software (SpectraMagic NX, Konica Minolta Corp., Ramsey, NJ), daylight illuminant (D65), and a viewing angle of 10° was used for measurement. Color coordinates were measured in CIElab color space. Each disc was placed on top of a calibrated white backing tile, measurements were taken by centering the measuring port over the discs, and the procedure repeated with a calibrated black tile serving as the background. All measurements were performed before and after outdoor weathering, with measurements performed on the same surfaces before and after weathering.

Translucency parameter (TP) was calculated as the three-dimensional color difference vector between measurements obtained on white and black backgrounds as follows (Johnston et al., 1995):

$$TP = [(L_B^* - L_W^*)^2 + (a_B^* - a_w^*)^2 + (b_B^* - b_W^*)^2]^{1/2}$$

Where the L^* axis is white-black, the a^* axis is red-green, the b^* is the yellow-blue, the subscript B refers to the black backing color parameter, and the subscript W refers to the white backing color parameter.

3.2.5 Viscoelastic Properties Measurement

Viscoelastic properties were measured using a Dynamic Mechanical Analyzer (DMA) (DMA 8000, Perkin Elmer, Inc., Waltham, MA) in tensile mode. This test was performed to determine elastic and damping properties of the PDMS formulations. The experiments were carried out in tension at a frequency of 1.0 Hz with 0.02 mm displacement in the temperature range between -150°C and 20°C, at a heating rate of 2 °C /min. The temperature range was chosen based on preliminary tests that identified

key thermal transitions. Rectangular samples 5 mm length x 6.3 mm width x 2.5 mm thickness were tested for storage modulus, loss modulus, and tan delta (n=3 per group). The storage modulus determined the elastic behavior of the elastomer and the ratio of the loss modulus to the storage modulus (tan delta) was a measure of the energy dissipation of a material, or its damping (Menard, 2008).

3.2.6 Microscopic analysis

To obtain the microscopic characterization and dispersion of the nanoparticle fillers, scanning electronic microscopy (SEM) was used to observe the bulk surface of the specimen. The samples were taken from approximately 1 mm thick elastomer sections for each of the three filler types. Prior to SEM examination, the samples were placed into a vacuum desiccator with silica gel desiccant for seven days. Then, the samples were sectioned into smaller sizes for placement onto SEM stubs with the sectioned surface facing the electron beam. The images were taken using SEM (Helios NanoLab 660, Thermo Fisher Scientific) at 500 times and 50,000 times magnification, with 2.0 kV acceleration voltage.

3.3 Data Analysis

For tensile properties, group means and standard errors were calculated for dependent variables ultimate tensile strength, elastic modulus, and failure strain, while independent variables were filler type (KH220, Uncoated and TS530) and filler loading (0%, 0.5%, 5%, 10%, and 15%). Each of the groups consisted of 12 samples, therefore, total samples that used in this test were 12 samples x 3 filler types x 5 filler loading = 180 samples. The null hypothesis was that tensile properties were not affected by filler type and filler loadings. This was tested by two-way ANOVA with Tukey post hoc test at $p<0.05$ level of confidence.

For tear strength, group means and standard errors were calculated for the dependent variable tear strength, while independent variables were filler type (KH220, Uncoated and TS530) and filler loading (0%, 0.5%, 5%, 10%, and 15%). Each of the groups consisted of 10 samples, therefore, total sample numbers were 10 samples x 3 filler types x 5 filler loading = 150 samples. The null hypothesis was that tear strength was not affected by filler type and filler loadings. This was tested by two-way ANOVA with Tukey post hoc test at $p<0.05$ level of confidence.

For durometer hardness and translucency parameter, group means and standard errors were calculated for dependent variables (hardness and translucency parameter). Independent variables were filler type (KH220, Uncoated and TS530), filler loading (0, 0.5, 5, 10, and 15%), weathering exposures (indoor and outdoor), and weathering time (before and after 3000 hours). Each of the groups consisted of 10 samples, then these samples were divided into 5 samples per indoor and outdoor group. Therefore, total samples tested were 150. The null hypothesis tested was that hardness and translucency parameters were not affected by filler type, filler loading, weathering exposure, and time. This was tested by four-way ANOVA with Tukey post hoc test at $p<0.05$ level of confidence.

Chapter 4: Results

4.1 Nanoparticle Dispersion

The dispersion of nanoparticles at 15% filler loadings was assessed from Scanning Electron Microscopy (SEM) micrographs. This filler loading was chosen because it was expected to be the most difficult to disperse and would permit the easiest SEM observation. The dispersion of KH220 filler particles is shown in Fig. 4.1 and 4.2 with 500x and 50,000x magnification, respectively. From Fig. 4.1, the images show that the filler particles are dispersed evenly in PDMS and with few agglomerates. A more detailed view of particle size and distribution can be observed at higher magnification in Fig. 4.2, where approximately 15 to 50 nm particles diameters are evident.

Uncoated filler particles showed uneven dispersion compared to KH220 particles (Fig. 4.3 and 4.4). In Fig. 4.3, at 500x magnification, certain particles appear as 1 to 10 μm-sized diameter clumps, indicative of particle agglomeration. At 50,000x magnification, a 1.5 μm-sized aggregate appears to contain particles ranging from approximately 15 nm to 300 nm in diameter (Fig. 4.4).

Figures 4.5 and 4.6 show dispersion of TS530 submicron fillers. Filler particles are evenly distributed in polymer, as shown at 800x magnification in Fig. 4.5. However, fewer particle numbers are observed compared to KH220 and uncoated nanoparticles. Particle sizes estimated from the micron marker present in Fig. 4.6, demonstrate 150 to 200 nm size particles.

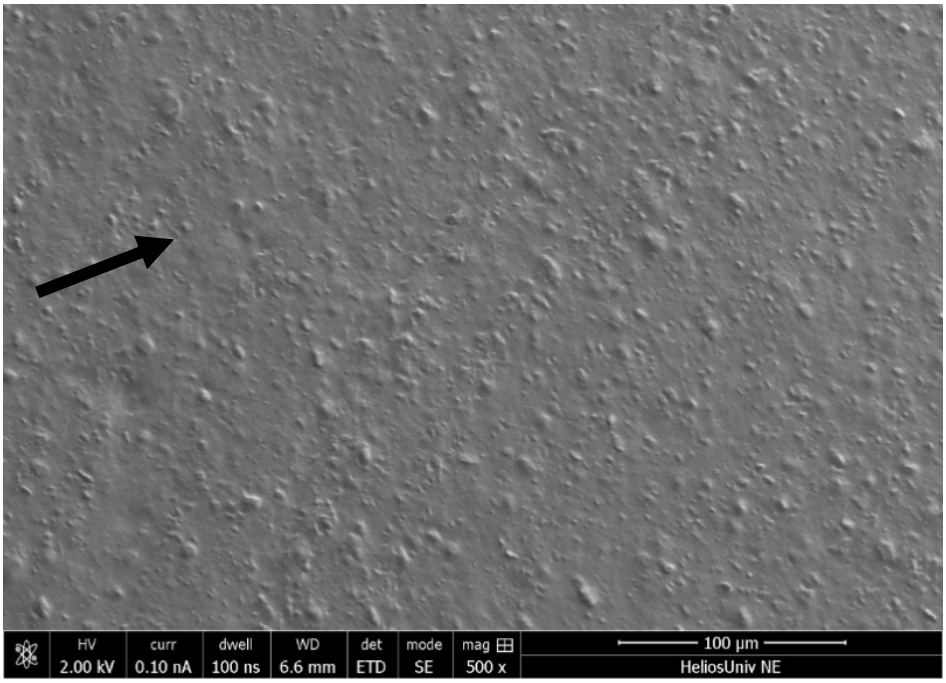

Figure 4.1 Dispersion of 15% KH220 filler loading at 500x magnification. Nanoparticles appear to be evenly distributed into the polymer. Arrow indicates a nanoparticle.

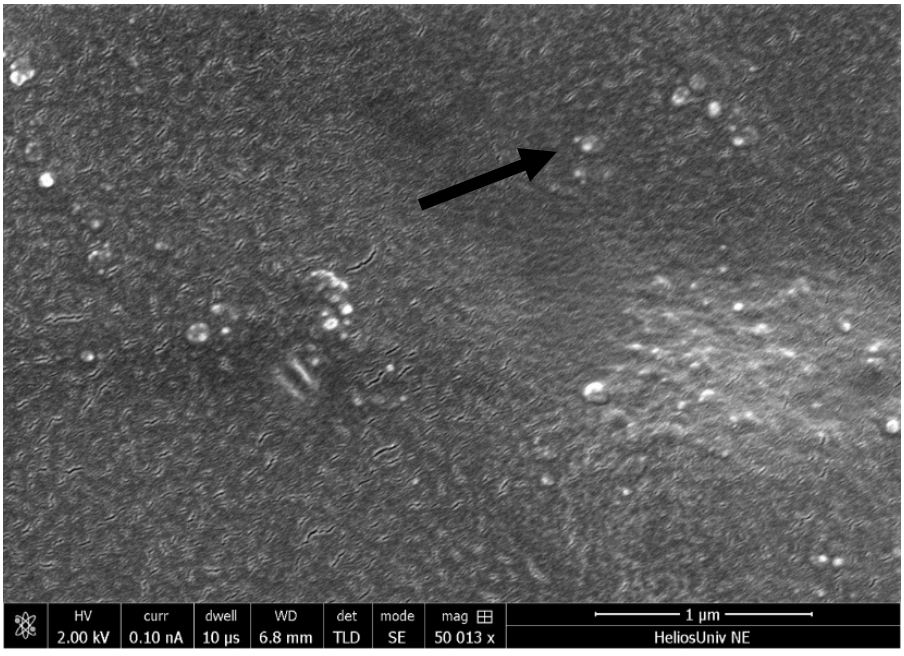

Figure 4.2 Dispersion of 15% KH220 filler loading at 50,000x magnification. Arrow points to a nanofiller particle approximately 20 nm diameter.

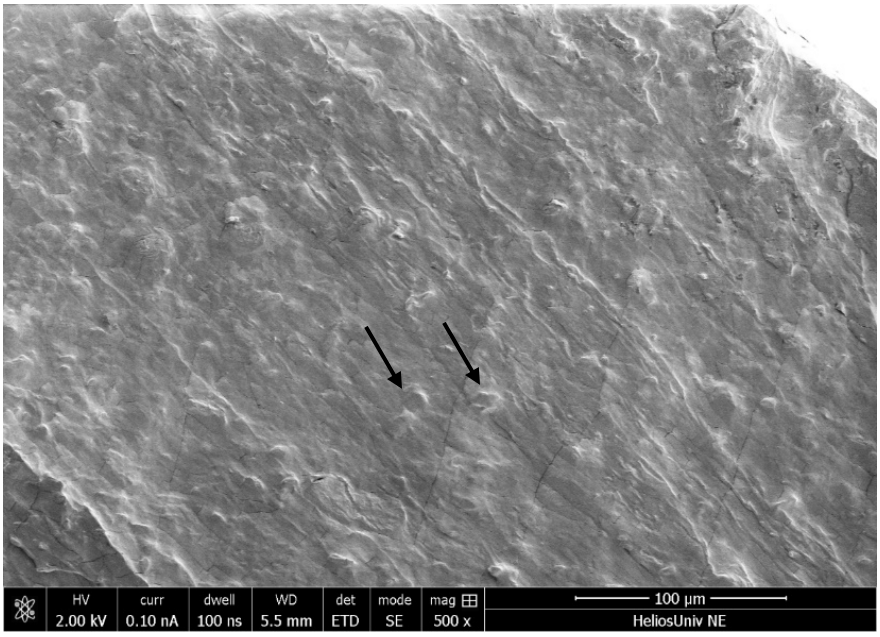

Figure 4.3 Dispersion of 15% Uncoated Filler loading at 500x magnification. Arrows indicate agglomeration of nanoparticles. A large number of aggregates can be seen throughout the polymer.

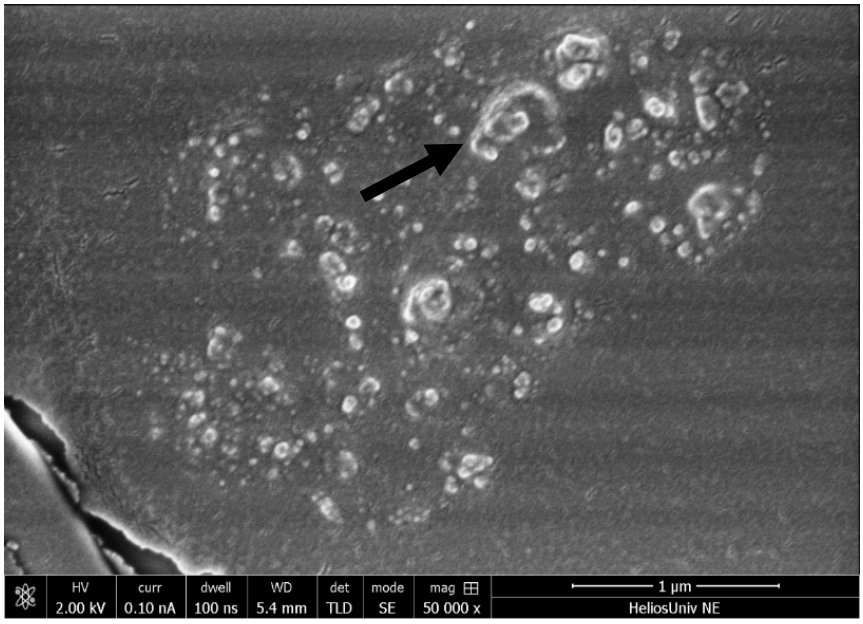

Figure 4.4 Dispersion of 15% Uncoated Filler loading at 50,000x magnification. Image demonstrates up to 0.4 μm diameter agglomerated nanoparticles (arrow), which are approximately 20 times larger than nanoparticles observed in Fig 4.2.

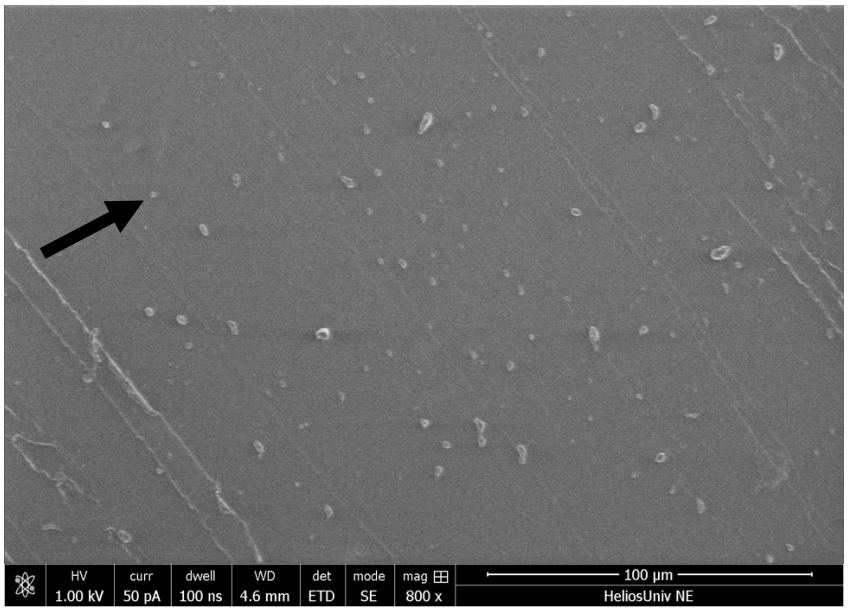

Figure 4.5 Dispersion of 15% TS530 filler loading at 800x magnification. Particles appear to be evenly distributed into the polymer, however, fewer particles are observed compared to nanofillers with similar magnifications. Arrow indicates submicron particle.

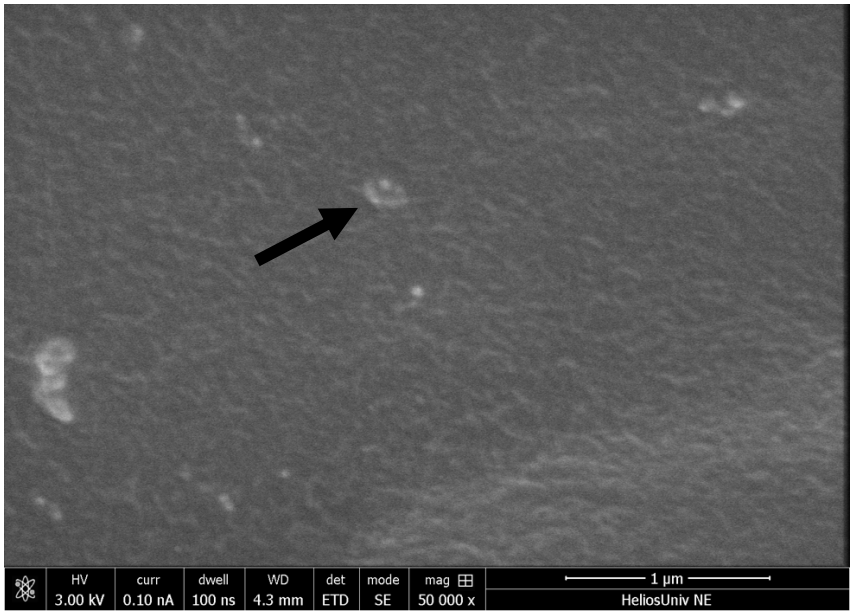

Figure 4.6 Dispersion of 15% TS530 filler loading at 50,000x magnification. Arrow points to filler particle approximately 200 nm in diameter.

4.2 Physical Properties

4.2.1 Tensile Properties

4.2.1.1 Tensile Strength

Plots of tensile strength versus weight percent filler for each group are presented in Fig. 4.7, and P-values from pairwise comparisons appear in Table 4.1. For all groups, the tensile strength increased non-linearly as filler content increased.

Tensile strength values among the three filler types were not significantly different at lower filler loadings (0% and 0.5%, $p \geq 0.05$). At 5% loadings and above, KH220-filled materials were significantly stronger than those filled with TS530, and stronger than Uncoated at 15% filler loading (all $p < 0.05$, Fig. 4.7, Table 4.1). No significant differences in tensile strength were noted at any filler loading between uncoated- and TS530-filled materials ($p \geq 0.05$). The highest tensile strength was recorded for 15% filled KH220 materials, which were 1.4 times higher than 15% uncoated-filled material and 1.3 times higher than 15% TS530-filled materials. Compared to unfilled PDMS, 15% KH220-, uncoated-, and TS530-filled materials were 6, 4.3, and 4.2 times stronger, respectively.

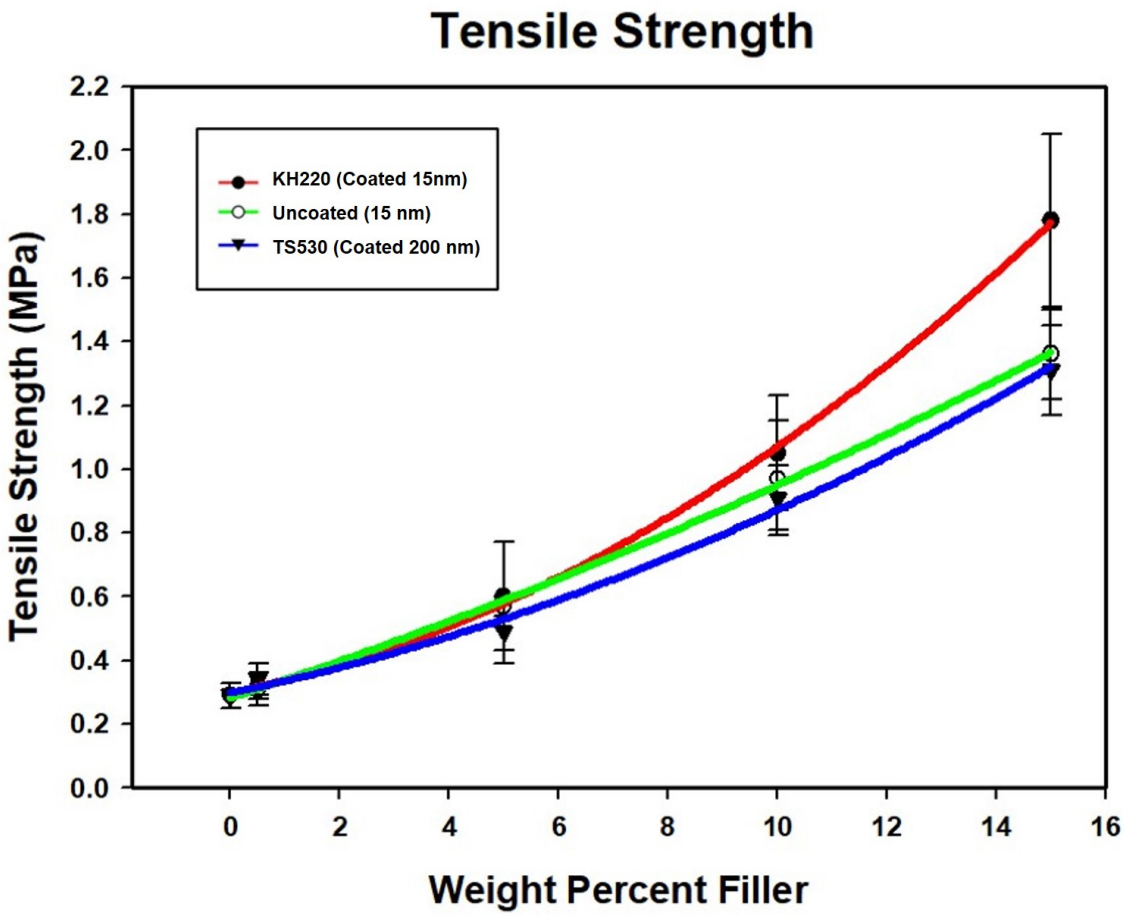

Figure 4.7 Plots of Tensile Strength (MPa) Versus Weight Percent Filler For Three Filler Types. Error Bars Represent Standard Errors of Means.

Table 4.1 P-Values From Pairwise Comparisons For Tensile Strength. Results From ANOVA/Tukey.

Group Comparisons for Tensile Strength*				
Weight Percent	Filler	KH220	Uncoated	TS-530
0.5%	KH220		p= 0.7580	
	Uncoated			P= 0.5380
	TS-530	P= 0.7580		
5%	KH220		P= 0.4956	
	Uncoated			P=0.1406
	TS-530	p= 0.0354		
10%	KH220		P= 0.0944	
	Uncoated			P=0.2932
	TS-530	p=0.0076		
15%	KH220		p<0.0001	
	Uncoated			P=0.3207
	TS-530	p<0.0001		

* Yellow boxes denote significantly different comparisons at the p<0.05 confidence level.

4.2.1.2 Elastic Modulus

Plots of elastic modulus versus weight percent filler loading are presented in Fig. 4.8, and P-values from pairwise comparisons are presented in Table 4.2. Results presented in Fig. 4.8 show non-linear elastic moduli increases for KH220- and uncoated-filled materials, whereas modulus values reached a plateau at 10 weight percent filler for TS530-filled elastomers.

Mean elastic modulus values among the three types of filler were not significantly different at low filler loadings (0% and 0.5%, $p \geq 0.05$), but above 5%, elastic modulus, KH220- and Uncoated-filled materials were significantly greater than TS530 materials ($p<0.05$). No significant differences in modulus were observed between KH220- and uncoated-filled materials until filler loadings reached 10% and 15% ($p<0.05$).

TS530-filled materials maintained lower elastic modulus values throughout all filler loading increases. At 5% loading, TS530-filled samples produced 1.3 times lower elastic modulus than both KH220- and uncoated-filled samples, and the gap widened at higher filler loadings. The highest mean elastic modulus was recorded for 15% KH220-filled materials, which were 1.5 times higher than uncoated-filled materials and 2.5 times higher than TS530-filled materials. KH220-, uncoated- and TS530-filled materials at 15% loading were 4.0, 3.5, and 1.7 times stiffer than unfilled PDMS, respectively.

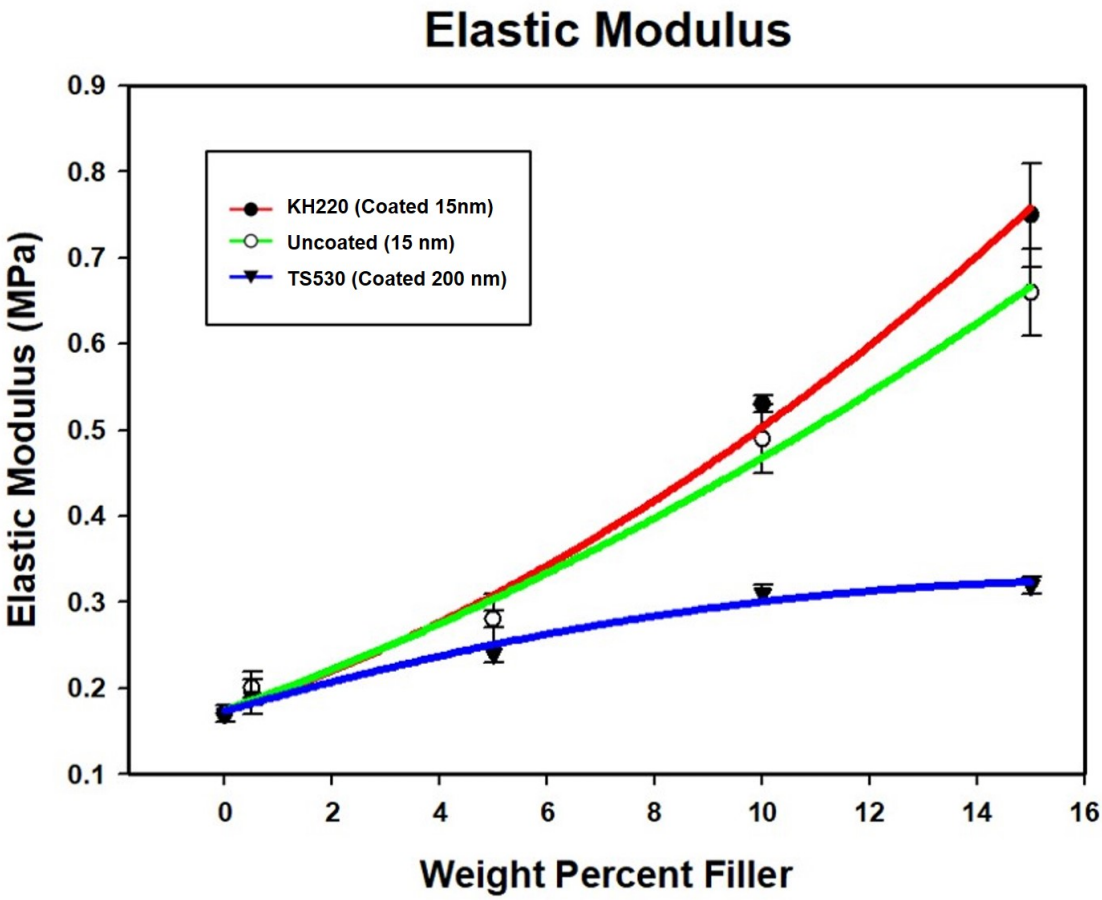

Figure 4.8 Plots of Mean Elastic Modulus (MPa) Versus Weight Percent Filler For Three Filler Types. Error Bars Represent Standard Errors of Means.

Table 4.2 P-Values From Pairwise Comparisons For Elastic Modulus. Results From ANOVA/Tukey.

Group Comparisons for Elastic Modulus*				
Weight Percent	Filler	KH220	Uncoated	TS-530
0.5%	KH220		P=0.8252	
	Uncoated			P=0.2398
	TS-530	P=0.3392		
5%	KH220		P=0.5560	
	Uncoated			p< 0.0001
	TS-530	P=0.0005		
10%	KH220		p< 0.0001	
	Uncoated			p< 0.0001
	TS-530	p< 0.0001		
15%	KH220		p<0.0001	
	Uncoated			p< 0.0001
	TS-530	p<0.0001		

* Yellow boxes denote significantly different comparisons at the p<0.05 confidence level.

4.2.1.3 Failure Strain

Plots of failure strain versus weight percent filler and P-values from pairwise comparisons are presented in Fig. 4.9 and Table 4.3. Results presented in Fig. 4.9 show failure strain changes for the three filler types as filler loading increases non-linearly. The trends were inverse compared to tensile strength and elastic modulus plots, where TS530-filled materials showed higher values than KH220- and uncoated-filled materials.

There were no significant differences of failure strain at lower filler loadings (0%, 0.5%, and 5%, $p<0.05$) for the three filler types, except between 0.5% uncoated- and TS530-filled materials ($p<0.05$). Failure strain of TS530-filled materials were significantly greater compared to KH220- and uncoated-filled materials for 10% and 15% filler loadings, while failure strain for 15% of KH220-filled materials were significantly greater than uncoated-filled materials ($p<0.05$).

The highest failure strain among all groups was for 15% TS530 filler, which was 1.4 times higher than 15% KH220-filled materials and 1.6 times higher than uncoated-filled materials. 15% filled KH220-, uncoated- and TS530-materials produced 2, 1.4, and 1.2 times strain to failure compared to unfilled PDMS, respectively.

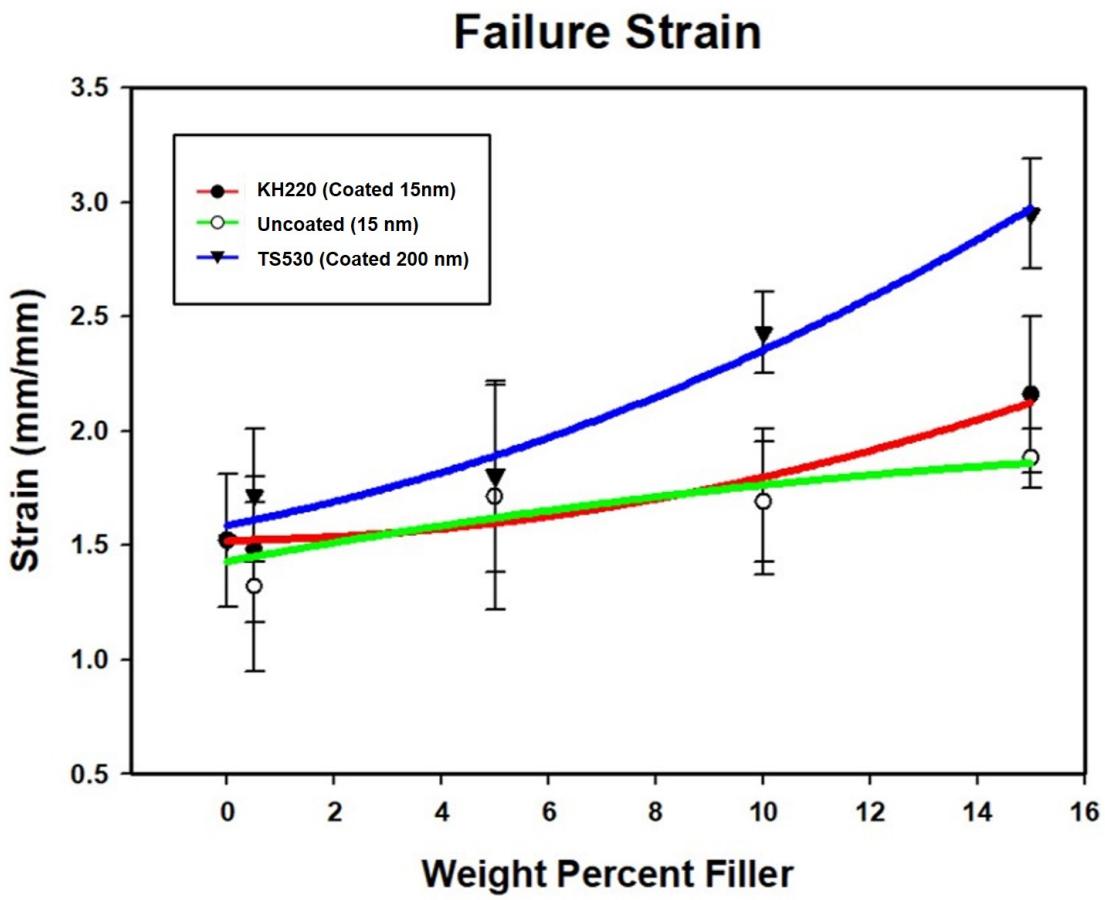

Figure 4.9 Plots of Failure Strain (mm/mm) Versus Weight Percent Filler For Three Filler Types. Error Bars Represent Standard Errors of Means.

Table 4. 3 P-Values From Pairwise Comparisons For Failure Strain. Results From ANOVA/Tukey.

Group Comparisons for Failure Strain*				
Weight Percent	Filler	KH220	Uncoated	TS-530
0.5%	KH220		P=0.1671	
	Uncoated			P=0.001
	TS-530	P=0.0514		
5%	KH220		P=0.9941	
	Uncoated			P=0.4404
	TS-530	P=0.4450		
10%	KH220		P=0.9743	
	Uncoated			p< 0.0001
	TS-530	p< 0.0001		
15%	KH220		P=0.0213	
	Uncoated			p< 0.0001
	TS-530	p<0.0001		
* Yellow boxes denote significantly different comparisons at the p<0.05 confidence level.				

4.2.2 Tear Strength

Plots of tear strength versus weight percent are presented in Fig. 4.10 and P-values from pairwise comparisons are presented in Table 4.4. Like tensile strength, tear strength for the three filler types increased in a non-linear manner as filler content increased. No significant differences in tear strength were noted at lower filler loadings (0%, 0.5%, and 5%, $p<0.05$) for the three types of filled materials. Tear strength of KH220 was significantly greater than uncoated and TS530 at 10% and 15% loadings, while tear strength of 10% filled TS530 was greater than uncoated at 10% loadings ($p<0.05$), but not significantly different at 15% load levels ($p\geq0.05$). The highest tensile strength was recorded for 15% filled KH220 materials, which were 1.2 and 1.3 times higher than 15% uncoated- and TS530-filled materials, respectively. Compared to unfilled PDMS, 15% KH220-, uncoated- and TS530-filled materials were 5.8, 4.8, and 4.4 times stronger, respectively.

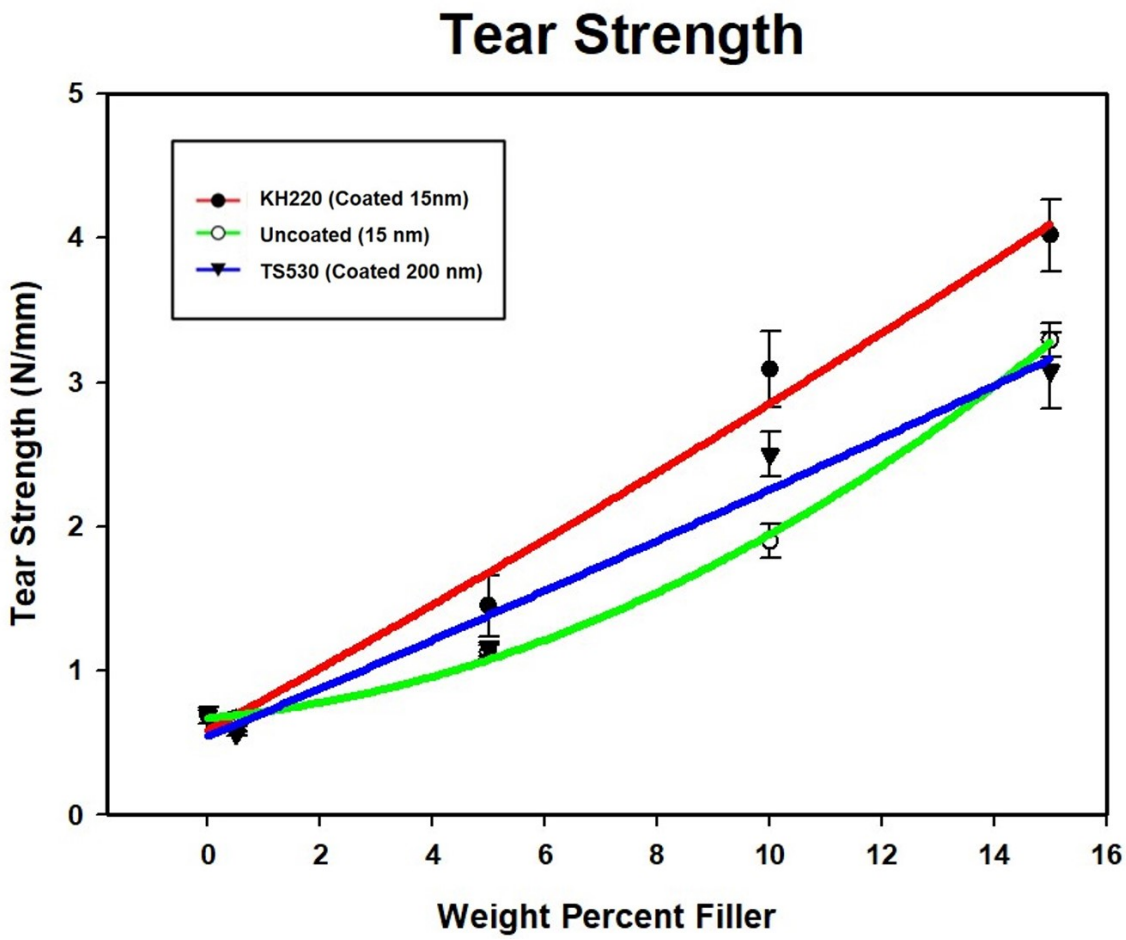

Figure 4.10 Plots of Tear Strength (N/mm) Versus Weight Percent Filler For Three Filler Types. Error Bars Represent Standard Errors of Means.

Table 4.4 P-Values From Pairwise Comparisons For Tear Strength. Results From ANOVA/Tukey.

Group Comparisons for Tear Strength*				
Weight Percent	Filler	KH220	Uncoated	TS-530
0.5%	KH220		P=0.9338	
	Uncoated			P=0.6549
	TS-530	P=0.5962		
5%	KH220		P=0.1224	
	Uncoated			P=0.9087
	TS-530	P=0.1523		
10%	KH220		p< 0.0001	
	Uncoated			p= 0.0038
	TS-530	P=0.0043		
15%	KH220		P= 0.0006	
	Uncoated			P=0.3119
	TS-530	p<0.0001		

* Yellow boxes denote significantly different comparisons at the p<0.05 confidence level.

4.2.3 Shore A Durometer Hardness

Figure 4.11 shows hardness differences among indoor groups before and after 3000 hours. As observed for other properties, hardness increased non-linearly with increasing filler levels for the three filler types. For indoor storage there were no differences in hardness before and after 3000 hours for all filler loadings and filler types, except for 15% loaded TS530 materials, which increased approximately 3 Shore A units ($p < 0.05$).

Hardness results for outdoor weathering appear in Fig. 4.12, and similar patterns with indoor groups were observed. No differences in hardness before and after weathering were noted, except for 10% and 15% loaded TS530 elastomers ($p<0.05$). These represented 2.6 and 2.4 hardness unit increases, respectively. The highest durometer hardness occurred with 15% KH220-filled materials, which were 1.2 times harder than 15% TS530-filled materials, but not significantly different from 15% uncoated-filled materials.

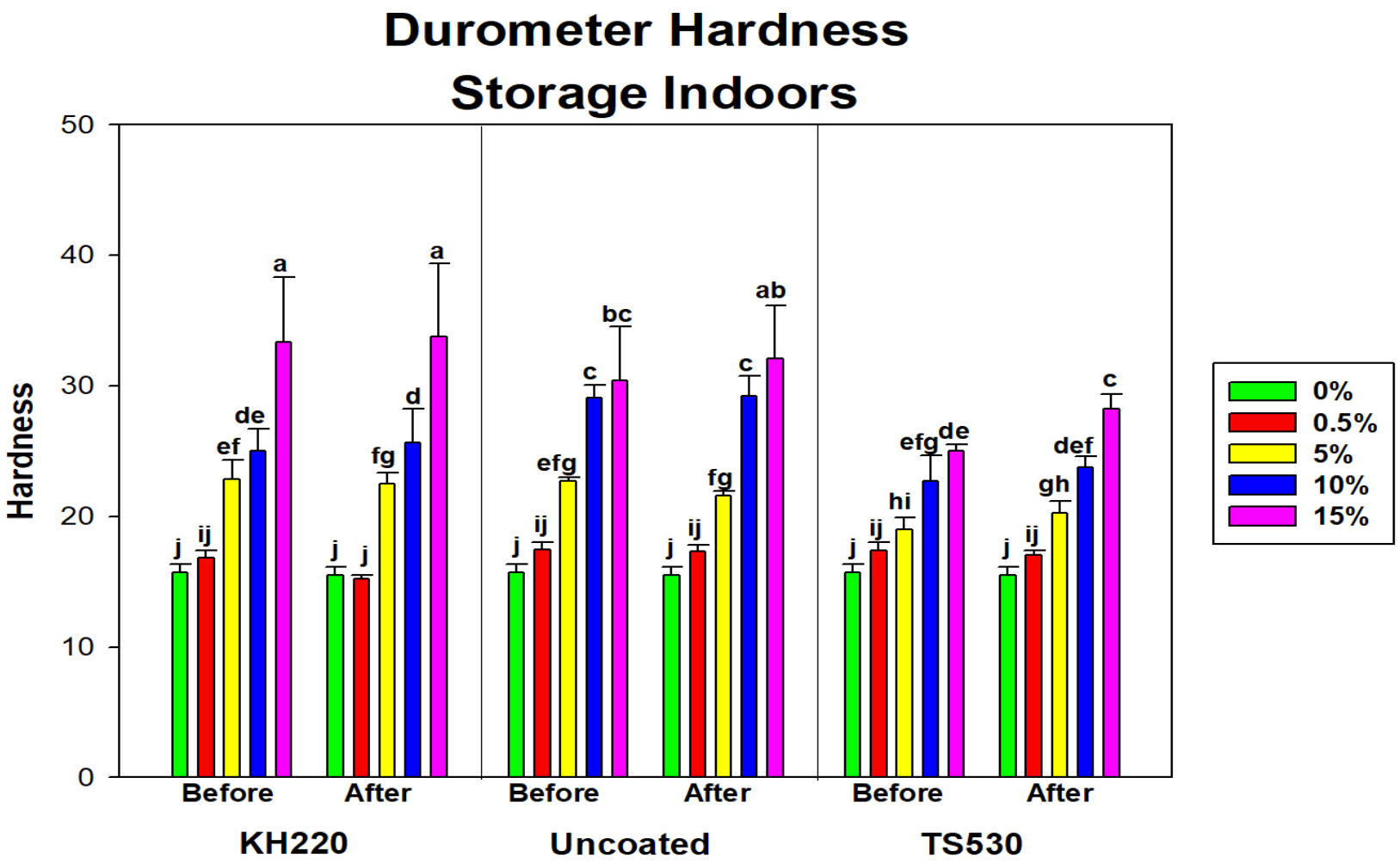

Figure 4.11 Bar graphs displaying means and error bars representing standard errors of means for Durometer Hardness for Indoor samples before and after 3000 hours of storage. Means with the same lowercase letters are not significantly different within and across groups ($p \geq 0.05$, ANOVA/Tukey).

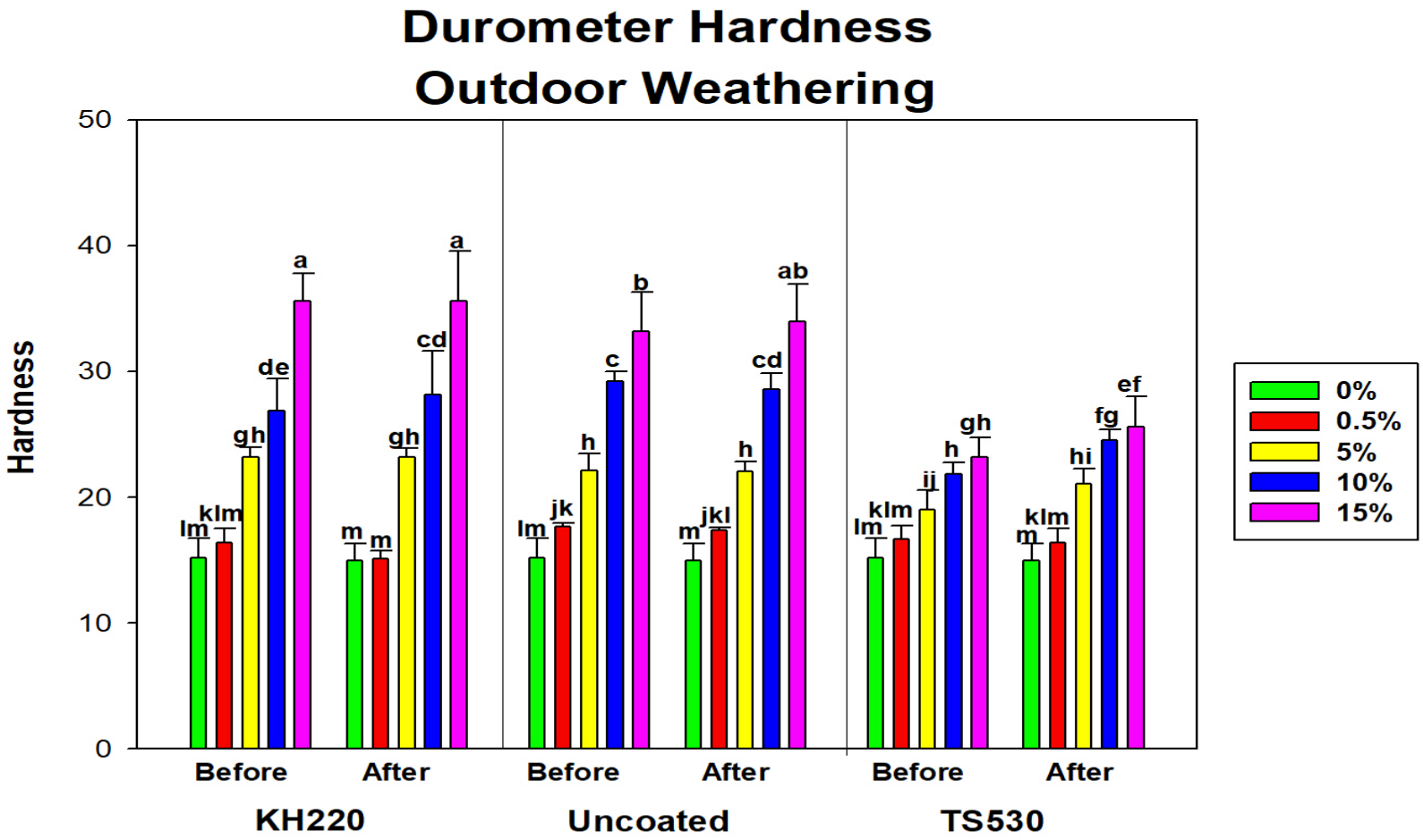

Figure 4.12 Bar graph displaying means and error bars representing standard errors of means for Durometer Hardness for Outdoor samples before and after 3000 hours of weathering. Means with the same lowercase letters are not significantly different within and across groups ($p \geq 0.05$, ANOVA/Tukey)

4.2.4 Translucency Parameter

Translucency parameter was calculated from L* a* b* differences measured on black and white backgrounds. Figure 4.13 displays translucency parameter values initially and following 3000 hours of indoor storage in darkness. No differences in translucency parameter were noted between before and after 3000 hours, regardless of filler loading or type ($p \geq 0.05$). There was a trend of decreasing translucency parameter values with each increase in filler loading for KH220- and uncoated-filled materials, but TS530 initially decreased, then remained unchanged at filler loadings above five weight percent.

Effects of outdoor weathering are shown in Fig. 4.14. All filler types experienced significant decreases in translucency for 0% and 0.5% filler content, which ranged from 50.91 to 45.03 and 44.96 to 39.24, respectively ($p<0.05$). Highly filled materials (10%, 15%) maintained translucency after outdoor weathering, with nanofilled materials possessing translucency parameter values 18 to 20 units lower than TS530-containing materials. From visual observation of the samples, lower filler loadings produced color changes that were darker and more opaque following 3000 hours of outdoor weathering, whereas undetectable color changes were observed in higher filled samples.

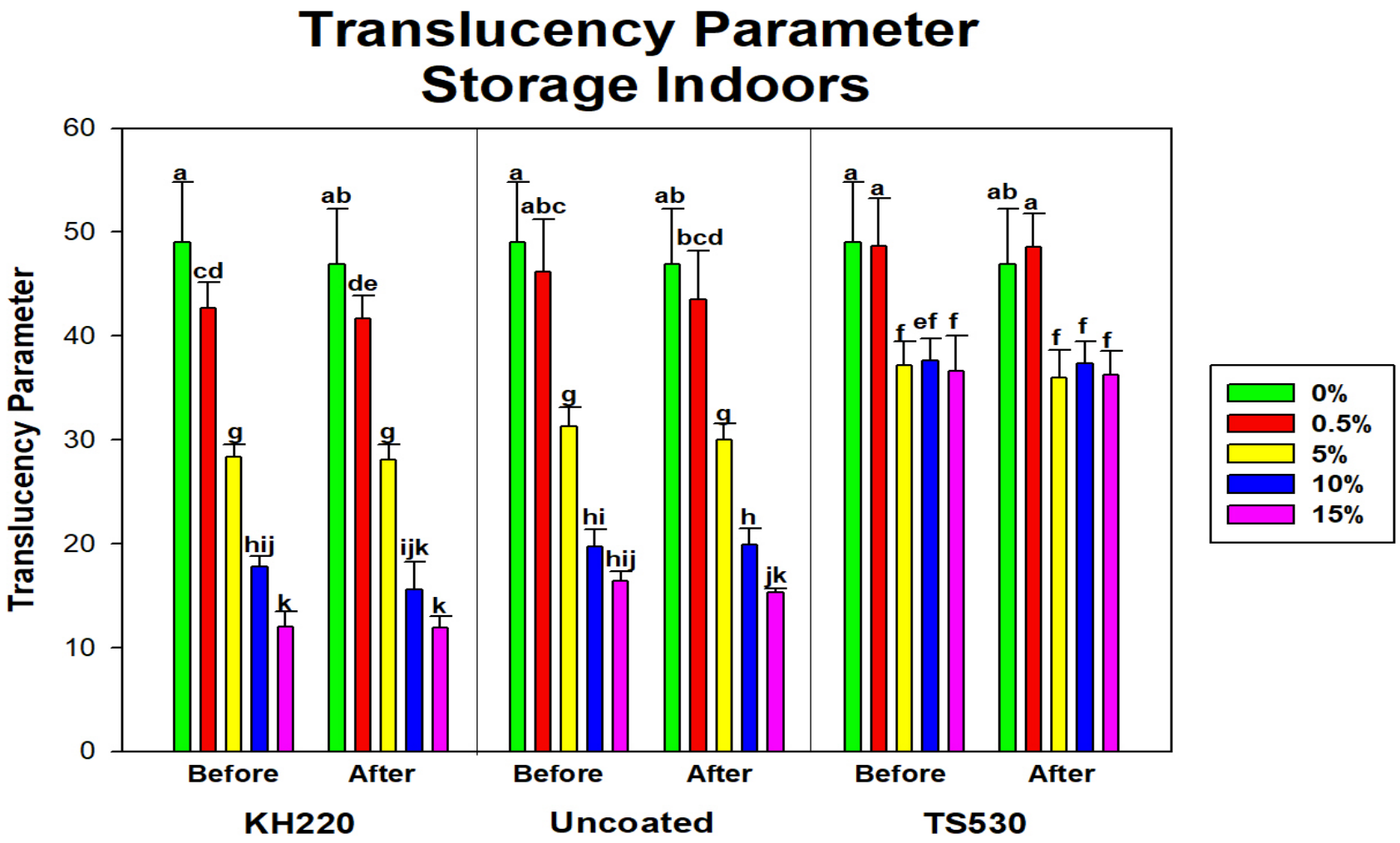

Figure 4.13 Bar graph displaying means and error bars representing standard error of Translucency Parameter for Indoor samples before and after 3000 hours of storage. Means with the same lowercase letters are not significantly different within and across groups ($p \geq 0.05$, ANOVA/Tukey).

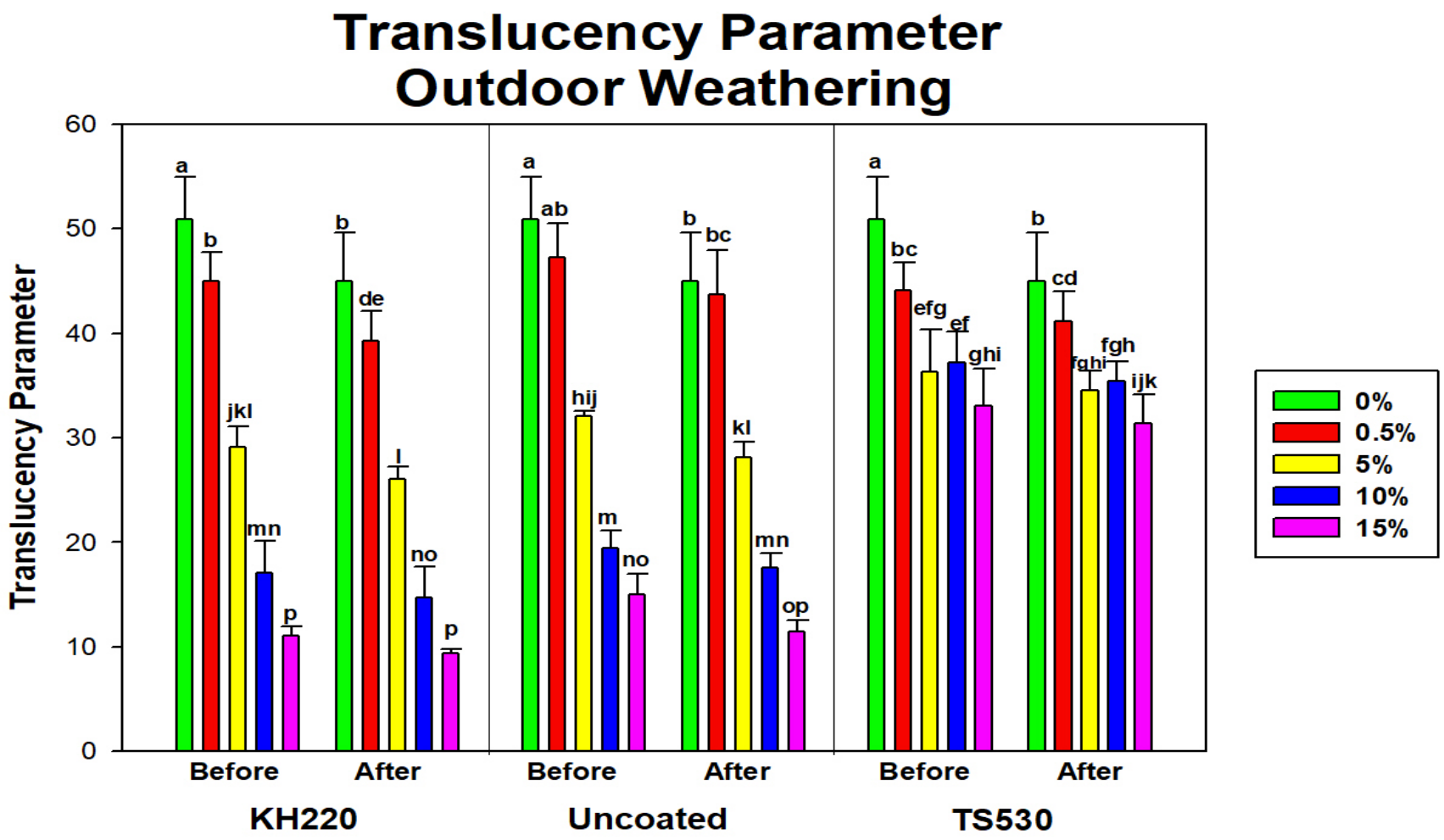

Figure 4.14 Bar graph displaying means and error bars representing standard errors of means for Translucency Parameter for Outdoor samples before and after 3000 hours of weathering. Means with the same lowercase letters are not significantly different within and across groups ($p \geq 0.05$, ANOVA/Tukey)

4.2.5 Viscoelastic Properties

Dynamic mechanical analysis (DMA) measures displacement response of materials when they are subjected to dynamic or cyclic forces. These responses are expressed in terms of storage modulus (elastic modulus, E'), loss modulus (viscous modulus, E''), and tan δ (damping coefficient, E''/E') as a function of temperature, frequency, or time. The storage modulus is a measure of a sample's elastic behavior, often associated with stiffness and is conceptually related to Young's modulus, however, they are not the same. Loss modulus is described as the dissipation of energy for a material under cyclic loading also known as damping. Glass transition (Tg) is the temperature indicating the relaxation in a polymer where a material changes from a glass to a rubber (Shrivastava, 2018).

Figures 4.15, 4.16, 4.17, and 4.18 show storage modulus, loss modulus and tan delta curves from unfilled, 15% coated nanosilica-, 15% uncoated nanosilica-, and 15% submicron silica-filled PDMS, respectively. A single peak was observed in E" and in tan delta, along with a drop of E', in all samples in the temperature region of the first glass transition, occurring between -110 to -95^{o}C (Transition I). At higher temperatures, -95 to -40^{o}C, E' and E" decreased gradually, with E' in 15% coated nanosilica-filled PDMS observed to have steeper curves compared to other groups. Additional tan delta peaks were observed at temperatures near -70^{o}C (Transition II) and -40^{o}C (Transition III). A rubbery plateau region was observed between -40^{o}C and +20^{o}C for all samples.

Table 4.5 show pairwise comparison for storage modulus, loss modulus, and tan delta. Three-way interaction of filler type, weight filler, and transition is significant in storage modulus ($p<0.05$), while there was no three-way interaction in loss modulus and tan delta ($p\geq0.05$). Tables 4.6, 4.8 and 4.10 show pairwise comparison results for storage modulus, loss modulus and tan delta for the three transitions, occurring at approximately -100^{o}C, -70^{o}C, and -40^{o}C. Filler type and weight percent filler had a

significant effect with storage modulus in Transition I and weight percent filler had a significant effect in tan delta at Transition II. Beside the above mentioned, filler type and weight percent filler exerted little effect on any of the viscoelastic properties at all three transition temperatures ($p \geq 0.05$). In the rubbery plateau region near room temperature (around 20^{o}C), both filler type and weight percent filler exerted significant differences on storage and loss moduli for the three filler types (Table 4.12, $p < 0.05$). The highest storage modulus, loss modulus, and tan delta values were recorded for the two 15%-nanoparticle-filled materials, approximately 1.1-1.4 MPa higher than unfilled and lowly filled PDMS. Storage modulus decreased after Transition I for all filler types.

Table 4.14 presents results from pairwise comparisons for primary glass transition temperatures occurring at Transition I. Tables 4.15 and 4.16 present results from pairwise comparisons for temperatures occurring at Transitions II and III, respectively. There was a significant effect of filler type and weight percent filler on Transition I and Transition II temperatures ($p < 0.05$). No significant differences were noted for Transition III temperatures ($p \geq 0.05$). All levels of filled PDMS demonstrated higher Transition I temperatures compared to unfilled PDMS. Transition I temperatures at all filler loadings were not significantly different between KH220- and TS530-filled materials, whereas KH220 was significantly higher than uncoated-filled materials at 5% and 10% filler loadings.

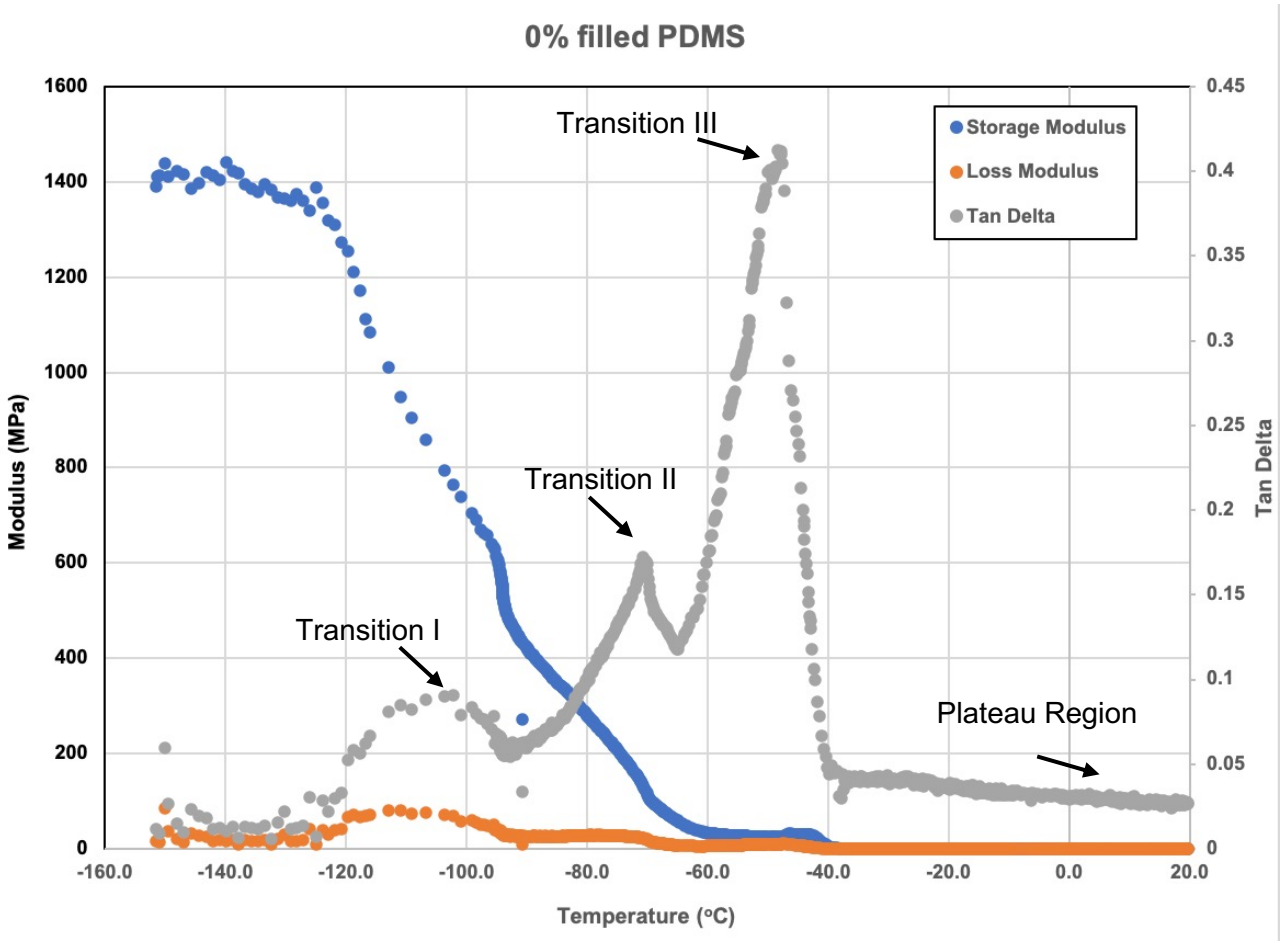

Figure 4.15 Storage Modulus, Loss Modulus, And Tan Delta Curves For 0% Filled PDMS From -150 °C To +20 °C.

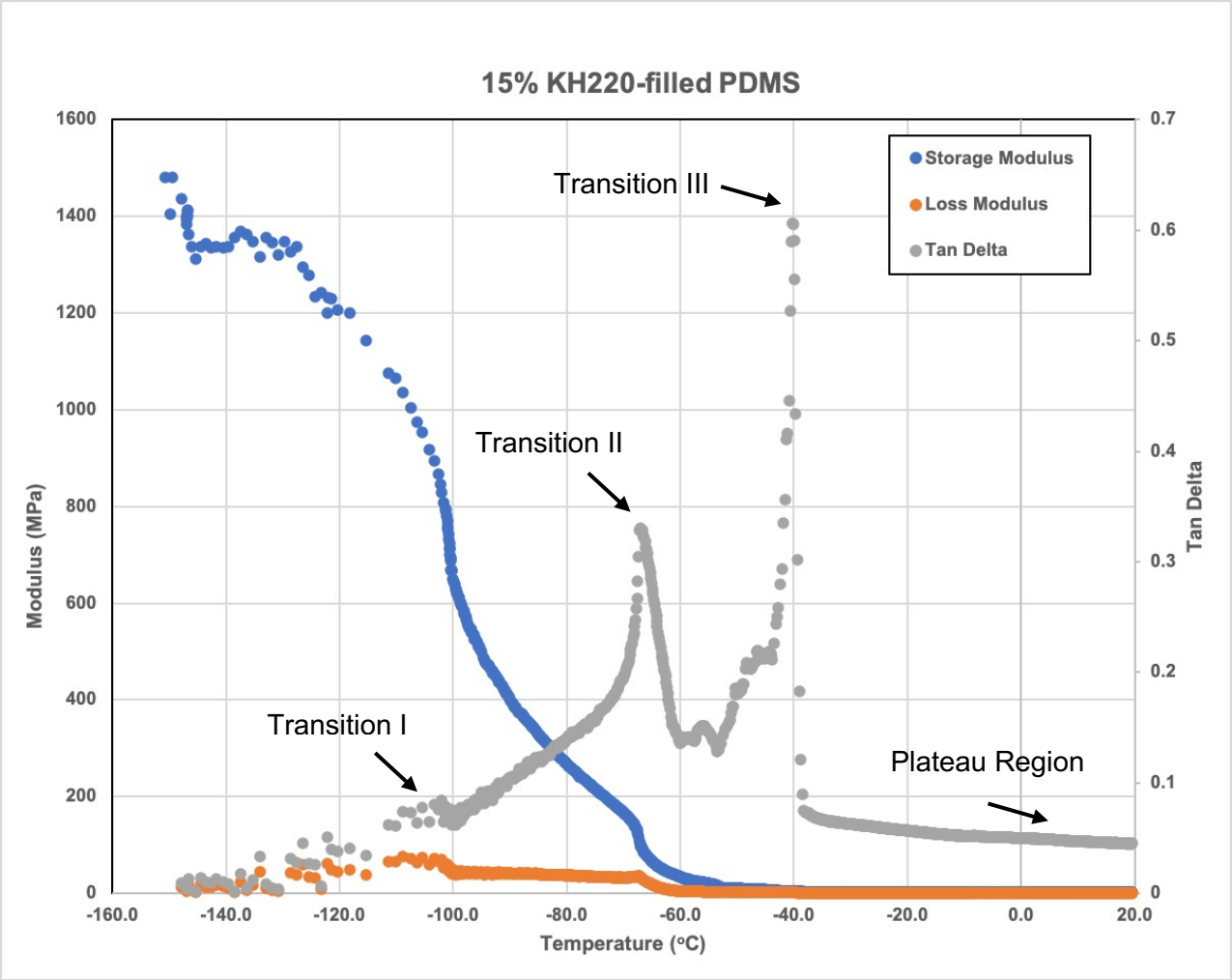

Figure 4.16 Storage Modulus, Loss Modulus, And Tan Delta Curves For 15% KH220-filled PDMS From -150 °C To +20 °C.

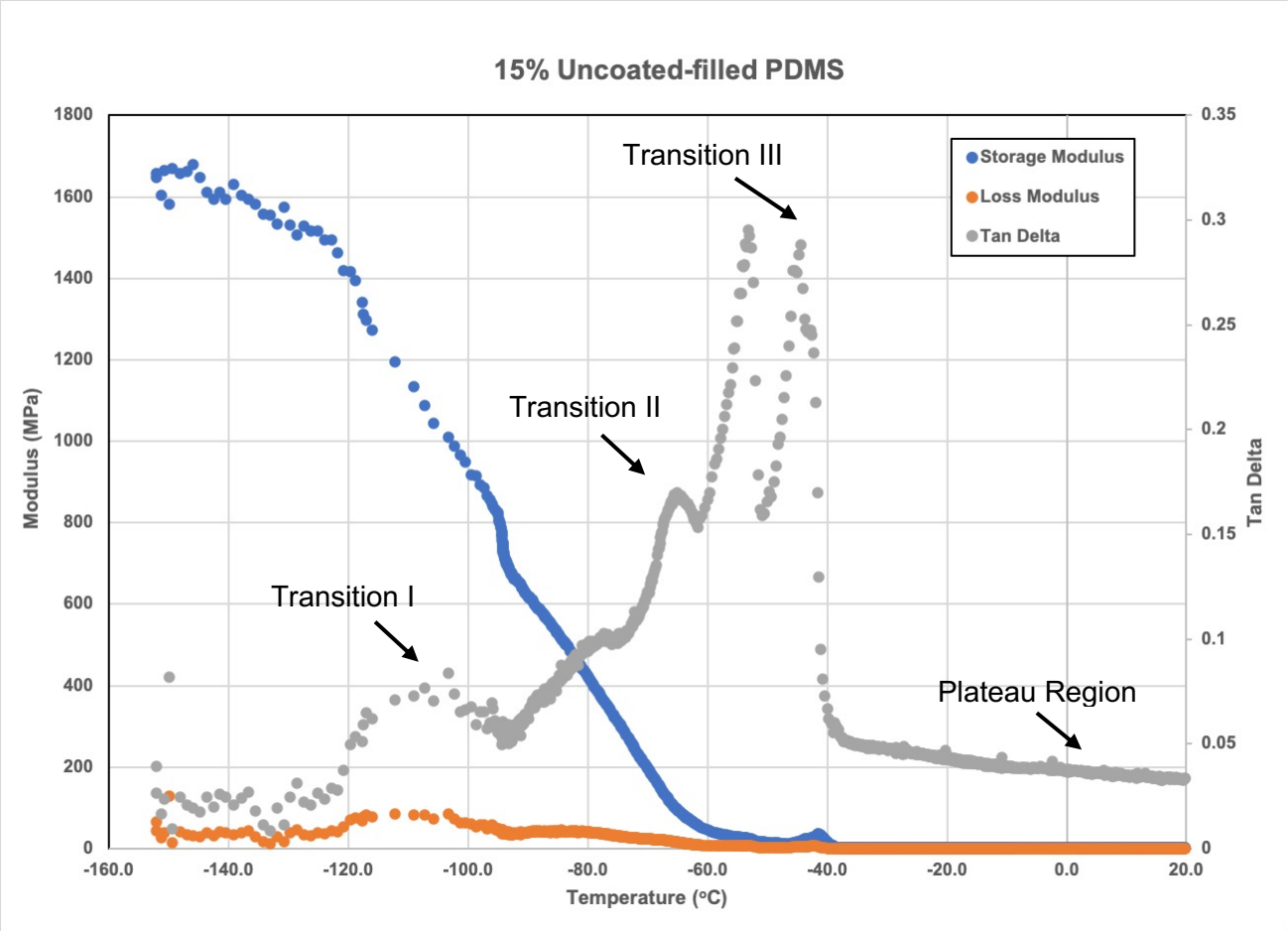

Figure 4.17 Storage Modulus, Loss Modulus, And Tan Delta Curves For 15% Uncoated-filled PDMS From -150 °C To +20 °C.

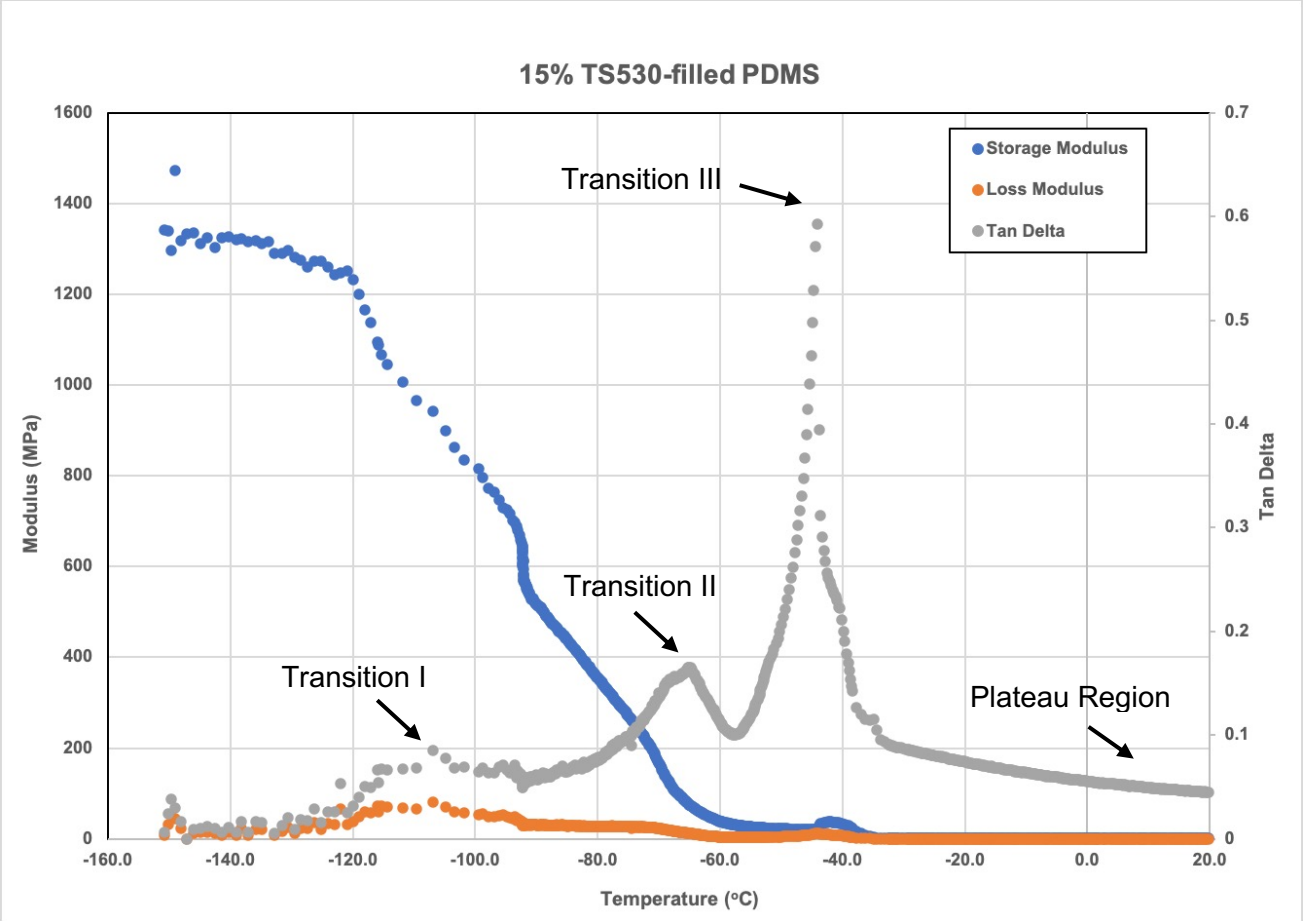

Figure 4.18 Storage Modulus, Loss Modulus, And Tan Delta Curves For 15% TS530-filled PDMS From -150 °C To +20 °C.

Table 4. 5 P-Values From Pairwise Comparisons For Storage Modulus, Loss Modulus And Tan Delta. Results From ANOVA/Tukey.

Three-Way ANOVA of Storage Modulus					
Source	**DF**	**Sum of Square**	**Mean Square**	**F Value**	**Pr > F**
Filler Type	2	15604.43	7802.21	0.75	0.4727
Weight Percent	4	61782.18	15445.55	1.49	0.2087
Weight Percent*Filler Type	8	335840.46	41980.06	4.06	0.0003
Transition	3	21381296.95	7127098.98	688.68	<.0001
Filler Type*Transition	6	40089.51	6681.58	0.65	0.6935
Weight Percent*Transition	12	172121.82	14343.48	1.39	0.1817
Filler*Weight*Transition	24	556545.00	23189.37	2.24	0.0023

Three-Way ANOVA of Loss Modulus					
Source	**DF**	**Sum of Square**	**Mean Square**	**F Value**	**Pr > F**
Filler Type	2	3442.5093	1721.2546	0.84	0.4335
Weight Percent	4	8247.0760	2061.7690	1.01	0.4060
Weight Percent*Filler Type	8	22128.9412	2766.1177	1.35	0.2244
Transition	3	252976.5152	84325.5051	41.24	<.0001
Filler Type*Transition	6	7712.0040	1285.3340	0.63	0.7071
Weight Percent*Transition	12	24734.2928	2061.1911	1.01	0.4460
Filler*Weight*Transition	24	51042.9232	2126.7885	1.04	0.4228

Three-Way ANOVA of Tan Delta					
Source	**DF**	**Sum of Square**	**Mean Square**	**F Value**	**Pr > F**
Filler Type	2	0.00263545	0.00131772	0.16	0.8525
Weight Percent	4	0.12560815	0.03140204	3.81	0.0060
Weight Percent*Filler Type	8	0.12352665	0.01544083	1.87	0.0704
Transition	3	3.21995793	1.07331931	130.19	<.0001
Filler Type*Transition	6	0.00544787	0.00090798	0.11	0.9951
Weight Percent*Transition	12	0.14429388	0.01202449	1.46	0.1494
Filler*Weight*Transition	24	0.21620197	0.00900842	1.09	0.3623

Table 4.6 P-Values From Pairwise Comparisons For Storage Modulus, Loss Modulus And Tan Delta At Transition I Temperature (Around -100°C). Results From ANOVA/Tukey.

Two-Way ANOVA of Storage Modulus Transition I					
Source	**DF**	**Sum of Square**	**Mean Square**	**F Value**	**Pr > F**
Filler Type	2	41069.7982	20534.8991	0.58	0.5678
Weight Percent	4	187202.6622	46800.6656	1.31	0.2872
Weight Percent*Filler Type	8	817414.8587	102176.8573	2.87	0.0180

Two-Way ANOVA of Loss Modulus Transition I					
Source	**DF**	**Sum of Square**	**Mean Square**	**F Value**	**Pr > F**
Filler Type	2	10734.35661	5367.17831	0.66	0.5225
Weight Percent	4	32210.31740	8052.57935	1.00	0.4254
Weight Percent*Filler Type	8	71959.13980	8994.89248	1.11	0.3834

Two-Way ANOVA of Tan Delta Transition I					
Source	**DF**	**Sum of Square**	**Mean Square**	**F Value**	**Pr > F**
Filler Type	2	0.00786410	0.00393205	1.89	0.1683
Weight Percent	4	0.00755062	0.00188766	0.91	0.4717
Weight Percent*Filler Type	8	0.01300920	0.00162615	0.78	0.6215

Table 4.7 Mean±SE of Storage Modulus, Loss Modulus, And Tan Delta At Transition I Temperature

Filler Type	Weight Percent	Storage Modulus (MPa)	Loss Modulus (MPa)	Tan Delta
	0	833 ± 35^{BC}	76.9 ± 10.6	0.092 ± 0.0103
KH220	**0.5**	827 ± 96^{BC}	74.5 ± 5.96	0.090 ± 0.0037
	5	1050 ± 288^{AB}	98.6 ± 37.7	0.092 ± 0.0097
	10	892 ± 83^{ABC}	84.8 ± 5.1	0.095 ± 0.0033
	15	731 ± 157^{CD}	81.2 ± 9.71	0.116 ± 0.0382
Uncoated	**0.5**	924 ± 39^{ABC}	86.1 ± 5.27	0.093 ± 0.0038
	5	836 ± 70^{BC}	83.4 ± 13.8	0.099 ± 0.0142
	10	751 ± 15^{BCD}	87.6 ± 16.3	0.117 ± 0.0234
	15	866 ± 146^{BC}	77.6 ± 7.35	0.090 ± 0.0068
TS530	**0.5**	481 ± 252^{D}	67.5 ± 35.5	0.140 ± 0.0018
	5	740 ± 131^{BCD}	81.5 ± 4.40	0.112 ± 0.0154
	10	724 ± 110^{CD}	70.8 ± 4.59	0.099 ± 0.0087
	15	910 ± 149^{ABC}	82.3 ± 3.23	0.089 ± 0.0214

*Means with the same superscript letter are not significantly different ($p \geq 0.05$). Vertical comparisons only.

Table 4.8 P-Values From Pairwise Comparisons For Storage Modulus, Loss Modulus And Tan Delta At Transition II Temperature (Around -70°C). Results From ANOVA/Tukey.

Two-Way ANOVA of Storage Modulus Transition II					
Source	**DF**	**Sum of Square**	**Mean Square**	**F Value**	**Pr > F**
Filler Type	2	14409.95107	7204.97553	1.29	0.2888
Weight Percent	4	45917.27759	11479.31940	2.06	0.1107
Weight Percent*Filler Type	8	73649.12646	9206.14081	1.65	0.1513

Two-Way ANOVA of Loss Modulus Transition II					
Source	**DF**	**Sum of Square**	**Mean Square**	**F Value**	**Pr > F**
Filler Type	2	416.251252	208.125626	2.79	0.0775
Weight Percent	4	725.849053	181.462263	2.43	0.0693
Weight Percent*Filler Type	8	1127.167724	140.895966	1.89	0.0994

Two-Way ANOVA of Tan Delta Transition II					
Source	**DF**	**Sum of Square**	**Mean Square**	**F Value**	**Pr > F**
Filler Type	2	0.00010094	0.00005047	0.00	0.9965
Weight Percent	4	0.18585198	0.04646299	3.22	0.0260
Weight Percent*Filler Type	8	0.25459222	0.03182403	2.21	0.0558

Table 4.9 Mean±SE of Storage Modulus, Loss Modulus, And Tan Delta At Transition II Temperature.

Filler Type	Weight Percent	Storage Modulus (MPa)	Loss Modulus (MPa)	Tan Delta
	0	132 ± 25.8	21.8 ± 4.78	0.164 ± 0.0051
KH220	**0.5**	119 ± 38	18.6 ± 7.21	0.155 ± 0.0410
	5	248 ± 215	27.6 ± 11	0.148 ± 0.0860
	10	112 ± 26.7	22.5 ± 8.9	0.195 ± 0.0371
	15	48.5 ± 51.4	18.9 ± 15	0.499 ± 0.3169
Uncoated	**0.5**	142 ± 61.6	18.2 ± 3.39	0.139 ± 0.0396
	5	93.5 ± 24.7	18.1 ± 5.74	0.192 ± 0.0136
	10	54.2 ± 58	11.9 ± 6.38	0.319 ± 0.1524
	15	22.3 ± 3.68	7.91 ± 1.05	0.359 ± 0.0561
TS530	**0.5**	72.4 ± 84.1	12.3 ± 3.90	0.327 ± 0.2302
	5	144 ± 38.4	33.7 ± 7.77	0.242 ± 0.0755
	10	64.8 ± 82.7	11.3 ± 10.1	0.265 ± 0.1345
	15	171 ± 84.7	31.8 ± 17.6	0.181 ± 0.0216

Table 4.10 P-Values From Pairwise Comparisons For Storage Modulus, Loss Modulus And Tan Delta At Transition III Temperature (Around -40°C). Results From ANOVA/Tukey.

Two-Way ANOVA of Storage Modulus Transition III					
Source	**DF**	**Sum of Square**	**Mean Square**	**F Value**	**Pr > F**
Filler Type	2	213.355474	106.677737	0.47	0.6274
Weight Percent	4	776.226578	194.056645	0.86	0.4983
Weight Percent*Filler Type	8	1320.587996	165.073499	0.73	0.6620

Two-Way ANOVA of Loss Modulus Transition III					
Source	**DF**	**Sum of Square**	**Mean Square**	**F Value**	**Pr > F**
Filler Type	2	3.90508207	1.95254104	0.14	0.8659
Weight Percent	4	45.19003203	11.29750801	0.84	0.5124
Weight Percent*Filler Type	8	85.55617355	10.69452169	0.79	0.6133

Two-Way ANOVA of Tan Delta Transition III					
Source	**DF**	**Sum of Square**	**Mean Square**	**F Value**	**Pr > F**
Filler Type	2	0.00005337	0.00002668	0.00	0.9984
Weight Percent	4	0.07545194	0.01886298	1.15	0.3537
Weight Percent*Filler Type	8	0.07177642	0.00897205	0.55	0.8127

Table 4.11 Mean±SE of Storage Modulus, Loss Modulus, And Tan Delta At Transition III Temperature.

Filler Type	Weight Percent	Storage Modulus (MPa)	Loss Modulus (MPa)	Tan Delta
	0	26.6 ± 6.46	8.20 ± 1.58	0.321 ± 0.0998
KH220	**0.5**	9.06 ± 6.39	4.03 ± 3.02	0.409 ± 0.0798
	5	19.5 ± 16.6	5.40 ± 2.88	0.336 ± 0.1134
	10	26 ± 10.4	9.20 ± 5.00	0.335 ± 0.0804
	15	12.5 ± 8.90	5.44 ± 2.86	0.499 ± 0.1572
Uncoated	**0.5**	15.1 ± 6.01	6.67 ± 3.42	0.440 ± 0.1032
	5	14.3 ± 2.87	5.82 ± 1.67	0.414 ± 0.1251
	10	9.20 ± 6.69	3.70 ± 3.17	0.406 ± 0.1429
	15	14.1 ± 6.71	4.72 ± 2.50	0.333 ± 0.0487
TS530	**0.5**	31.2 ± 46.4	7.33 ± 8.25	0.482 ± 0.2536
	5	15.2 ± 2.41	5.15 ± 1.91	0.341 ± 0.1152
	10	10.4 ± 1.21	3.96 ± 4.13	0.382 ± 0.0344
	15	22.4 ± 21.3	7.52 ± 6.45	0.379 ± 0.1960

Table 4.12 P-Values From Pairwise Comparisons For Storage Modulus, Loss Modulus And Tan Delta At Plateau Region Temperature (Around 20°C). Results From ANOVA/Tukey.

Two-Way ANOVA of Storage Modulus Plateau Region					
Source	**DF**	**Sum of Square**	**Mean Square**	**F Value**	**Pr > F**
Filler Type	2	0.83030715	0.41515357	34.88	<.0001
Weight Percent	4	7.83491874	1.95872969	164.57	<.0001
Weight Percent*Filler Type	8	0.88693895	0.11086737	9.31	<.0001

Two-Way ANOVA of Loss Modulus Plateau Region					
Source	**DF**	**Sum of Square**	**Mean Square**	**F Value**	**Pr > F**
Filler Type	2	0.00036881	0.00018440	6.91	0.0034
Weight Percent	4	0.01231458	0.00307865	115.28	<.0001
Weight Percent*Filler Type	8	0.00069124	0.00008640	3.24	0.0090

Two-Way ANOVA of Tan Delta Plateau Region					
Source	**DF**	**Sum of Square**	**Mean Square**	**F Value**	**Pr > F**
Filler Type	2	0.00006491	0.00003246	1.36	0.2715
Weight Percent	4	0.00104750	0.00026187	10.99	<.0001
Weight Percent*Filler Type	8	0.00035078	0.00004385	1.84	0.1083

*Table 4.13 Mean±SE of Storage Modulus, Loss Modulus, And Tan Delta At Plateau Region. Results From ANOVA/Tukey**

Filler Type	Weight Percent	Storage Modulus (MPa)	Loss Modulus (MPa)	Tan Delta
	0	0.48 ± 0.018^{GH}	0.01 ± 0.024^{fg}	0.026 ± 0.0012^{CDEF}
KH220	**0.5**	0.52 ± 0.004^{GH}	0.01 ± 0.002^{fg}	0.026 ± 0.0047^{CDEF}
	5	0.72 ± 0.104^{EF}	0.02 ± 0.001^{def}	0.029 ± 0.0067^{CDEF}
	10	1.28 ± 0.082^{B}	0.03 ± 0.002^{c}	0.024 ± 0.0008^{DEF}
	15	1.82 ± 0.264^{A}	0.06 ± 0.016^{a}	0.038 ± 0.0134^{AB}
Uncoated	**0.5**	0.55 ± 0.001^{FGH}	0.02 ± 0.006^{fg}	0.030 ± 0.0106^{CDEF}
	5	0.78 ± 0.029^{DE}	0.02 ± 0.002^{ef}	0.024 ± 0.0013^{DEF}
	10	1.25 ± 0.067^{B}	0.03 ± 0.002^{cde}	0.022 ± 0.0014^{EF}
	15	1.85 ± 0.130^{A}	0.06 ± 0.005^{a}	0.033 ± 0.0003^{BC}
TS530	**0.5**	0.39 ± 0.253^{H}	0.009 ± 0.006^{g}	0.021 ± 0.0020^{F}
	5	0.64 ± 0.019^{EFG}	0.019 ± 0.001^{f}	0.029 ± 0.0012^{CDEF}
	10	0.92 ± 0.014^{CD}	0.028 ± 0.001^{cd}	0.030 ± 0.0005^{BCD}
	15	0.99 ± 0.059^{C}	0.043 ± 0.004^{b}	0.043 ± 0.0022^{A}

*Means with the same superscript letter are not significantly different ($p \geq 0.05$). Vertical comparisons only.

Table 4.14 P-Values From Pairwise Comparisons For Transition I Temperature. Results From ANOVA/Tukey.

Two-Way ANOVA of Transition I					
Source	**DF**	**Sum of Square**	**Mean Square**	**F Value**	**Pr > F**
Filler Type	2	15.25911111	7.62955556	4.21	0.0245
Weight Percent	4	47.53688889	11.88422222	6.55	0.0006
Weight Percent*Filler Type	8	14.46977778	1.80872222	1.00	0.4582

*Table 4.15 Mean±SE of Transition I Temperatures. Results From ANOVA/Tukey**

Filler Type	Weight Percent	Transition I (°C) Mean±SE
	0	-103.3 ± 0.64^{D}
KH220	0.5	-101.3 ± 1.16^{ABC}
	5	-99.8 ± 0.66^{A}
	10	-99.7 ± 1.39^{A}
	15	-99.8 ± 1.31^{A}
Uncoated	0.5	-101.4 ± 0.67^{ABCD}
	5	-102.3 ± 0.34^{BCD}
	10	-102.6 ± 1.93^{CD}
	15	-101.1 ± 2.20^{ABC}
TS530	0.5	-100.0 ± 2.07^{A}
	5	-101.3 ± 0.87^{ABCD}
	10	-100.5 ± 1.53^{ABC}
	15	-100.1 ± 1.59^{AB}

*Means with the same superscript letter are not significantly different ($p \geq 0.05$). Vertical comparisons only.

Table 4.16 P-Values From Pairwise Comparisons For Transition II Temperatures. Results From ANOVA/Tukey.

Two-Way ANOVA of Transition II					
Source	**DF**	**Sum of Square**	**Mean Square**	**F Value**	**Pr > F**
Filler Type	2	274.3093333	137.1546667	3.35	0.0487
Weight Percent	4	649.1475556	162.2868889	3.96	0.0107
Weight Percent*Filler Type	8	386.3617778	48.2952222	1.18	0.3438

*Table 4.17 Mean±SE of Transition II Temperatures. Results From ANOVA/Tukey**

Filler Type	Weight Percent	Transition II (°C) Mean±SE
	0	-67.6 ± 3.57^{A}
KH220	0.5	-68.5 ± 5.02^{A}
	5	-71.1 ± 1.01^{A}
	10	-73.2 ± 8.04^{AB}
	15	-65.8 ± 5.91^{A}
Uncoated	0.5	-67.3 ± 1.27^{A}
	5	-68.7 ± 4.01^{A}
	10	-75.2 ± 14.51^{ABC}
	15	-71.7 ± 8.96^{AB}
TS530	0.5	-67.3 ± 4.84^{A}
	5	-84.6 ± 3.50^{C}
	10	-82.4 ± 6.86^{BC}
	15	-65.8 ± 7.63^{AB}

*Means with the same superscript letter are not significantly different ($p \geq 0.05$). Vertical comparisons only.

Table 4.18 P-Values From Pairwise Comparisons For Transition III Temperature. Results From ANOVA/Tukey.

Two-Way ANOVA of Transition III					
Source	**DF**	**Sum of Square**	**Mean Square**	**F Value**	**Pr > F**
Filler Type	2	299.377333	149.688667	0.79	0.4614
Weight Percent	4	1196.134667	299.033667	1.59	0.2036
Weight Percent*Filler Type	8	1492.509333	186.563667	0.99	0.4637

Table 4.19 Mean±SE of Transition III Temperatures. Results From ANOVA/Tukey.

Filler Type	Weight Percent	Transition III (°C) Mean±SE
	0	-47.0 ± 4.78
KH220	0.5	-44.6 ± 3.65
	5	-47.6 ± 1.53
	10	-49.5 ± 3.53
	15	-43.7 ± 2.96
Uncoated	0.5	-47.3 ± 1.83
	5	-47.5 ± 2.33
	10	-46.7 ± 4.84
	15	-44.2 ± 0.75
TS530	0.5	-48.1 ± 5.39
	5	-44.2 ± 3.50
	10	-44.3 ± 2.07
	15	-43.4 ± 5.23

Chapter 5: Discussion

The central hypothesis of this study was that sequential additions of "superhydrophobic"-coated nano-SiO_2 to PDMS would generate improved physical properties compared to PDMS filled with uncoated nano-SiO_2 or conventional submicron SiO_2. Improvements desired were higher tensile strength, failure strain and tear strength, while maintaining lower elastic modulus and hardness. Results from this study demonstrated that highly filled materials containing coated nano-SiO_2 in PDMS produced the highest tensile strength and tear resistance, therefore the hypothesis was accepted for those properties. However, these materials also generated low strain to failure, high elastic modulus and high hardness. For these properties, the null hypothesis was rejected. Interpretation of results are presented in the following sections.

5.1 Tensile and Tear Properties

Compared to uncoated nano-SiO_2 or conventional submicron SiO_2, ultimate tensile strength and elastic modulus of superhydrophobic-coated nano-SiO_2 filled samples were greatest at 15% filler loading (roughly 1.3 – 1.4 times greater tensile strength, 1.5 – 2.5 times greater elastic modulus, Fig. 4.7 and 4.8). This was primarily attributed to high filler loadings and to properties attributed to nanoparticles. These include an increased number of particles per unit mass loaded into the polymer, increased surface reactivity and improved dispersion when coated with a hydrophobic compound.

It is well documented that increasing filler levels increase mechanical properties in polymer systems. In dental resin-based composites, properties such as compressive and tensile strengths, elastic modulus, hardness and wear resistance are increased

with sequential additions of micrometer and submicrometer size fillers. Water sorption and hydrolytic degradation are decreased (Hirasawa, 1963; St. Germain et al.,1985; Beatty et al., 1998). Similar results have been shown for filled PDMS systems, where tensile strength, tear strength, and hardness increase with the addition of nanometer size fillers (Zayed et al., 2014; Tukmachi et al., 2017).

In this study, tensile strength was 420% to 600% higher for the three 15% filled materials compared to unfilled PDMS. In unfilled polymer, applied tensile stress serves to straighten the polymer chains, and microvoids are formed as means to redistribute molecular voids in the polymer. These microvoids continue to grow into failure since voids act as stress concentrators which trigger the onset of failure at lower stresses (Lampman, 2003). In filled systems, silica fillers serve to reinforce the polymer by filling the voids. The substantially improved properties occur due to reinforcement encouraged by the silica's large surface area, and when hydroxyl groups on the filler surface form hydrogen bonds between the filler and Si and CH_2 in the siloxane polymer (Liu et al., 2012). This permits adsorption of filler to polymer molecules, better reinforcement under load, higher tensile strength and elongation capability (Lynch, 1978). In addition, reinforcement of PDMS is also contributed by particle-particle interaction, where hydrogen bonding between free hydroxyl groups on surface particles significantly increases the resistance to the applied force, and polymerization shrinkage decreases (Camenzind et al., 2010).

As mentioned, the ten-fold size reduction from submicron- to nano-sized particles increases surface area by approximately 1000 and decreases volume by approximately 1000, producing a surface area/volume ratio of 0.15, which is ten times higher. Assuming the same mass is present within materials loaded with the different particles, this roughly equates to ten times more nanoparticles per unit volume. The surface area/weight ratio increases by one to two orders of magnitude as the

nanoparticles decrease in size from 100 to 10 nm (Rothon, 2003). The increased particle numbers, in conjunction with a higher total surface area, provides more reinforcement sites with a more efficient stress transfer mechanism, which in turn increases strength (Fu et al., 2008). This underlies the differences observed in tensile strength and elastic modulus for 15%-filled PDMS compared to lower weight percentages.

Untreated silica fillers have moisture-attracting silanol groups (SiOH) on the surface which are formed as a result of rehydroxylation of silica when exposed to water or aqueous solutions. Even the presence of humidity readily populates the surfaces with hydroxyl groups. The presence of silanol groups increase electronegativity and renders a hydrophilic surface. The hydroxyl groups (OH^-) act as the centers of molecular adsorption and are capable of forming a hydrogen bond with other OH^- groups (Zhuravlev et al., 2000). This hydrogen bonding results in strong filler-filler attraction and tight aggregates can form, causing poor dispersion of silica into polymer (Choi et al., 2003). Hydrophobic coatings decrease the number of sites where silanol groups reside on the silica surface of silica, as silane coatings react with or displace the silanol groups. The net result is to reduce particle-particle attraction and hence agglomeration, which in turn promotes improved dispersion of filler into the uncured siloxane oligomer (Waters et al., 1996; Ray et al., 2004; Rahman et al., 2012). Unfortunately, when manufactured and stored as powders, the silica particles can agglomerate through condensation reactions at interparticle contacts that are generated during the drying process, which renders dispersibility more challenging (Rahman et al., 2012).

High speed rotary mixing successfully disperses submicron size silica into PDMS, whereas this is ineffective for nanosized silica. This is because surface activity of nanoparticles is high and requires higher forces to break apart particle agglomerates (Tanahashi et al., 2006). When filled PDMS is under external forces, the agglomerated

particles act as stress concentrating centers within the polymer matrix, thereby decreasing mechanical strength, which implies that the reinforcement is not efficient. When coated with a hydrophobic silane, improved dispersion and reduced base viscosity are realized (Zayed et al., 2014).

Two fillers contained hydrophobic coatings in this study. TS-530, the submicron size filler, was coated with hexamethyldisilazane (HMDS), while dimethoxydiphenyl silane (DMDPS, or KH220) served as the “superhydrophobic” coating for 15 nm particles. Chemical structures are provided in Figures 5.2 and 5.3, and chemical reactions for silane adsorptions onto silica are illustrated in Figs 5.4 and 5.5. The silylation of oxide surfaces normally involves reactions with surface hydroxyl groups that make up silanol sites. For TS530 silica, one mole HMDS reacts with two surface OH^- groups, generating two moles of trimethyl siloxane and releasing NH_3 as a by-product (Fig. 5.4). Hydrophobicity is imparted through the electropositive trimethylsilyl groups, which replace many of the negatively charged surface hydroxyl groups (Gun’ko et al., 2000). For DMDPS, silylation proceeds through hydrolysis of trimethoxy groups ($O(CH_3)_3$), followed by condensation to produce a silyl alcohol that is attracted to surface OH^- groups present on the silica surfaces. Further condensation removes water and produces covalent Si-O bonds (Fig. 5.5). Hydrophobicity is imparted by phenyl groups (R groups in Fig. 5.5) that replace condensed OH^- groups. It is important to note that one OH^- group remains on hydrolyzed DMDPS, which forms hydrogen bonds with the silica silanol, but also offers potential for attraction with Si and CH_2 present on the PDMS backbone.

In comparing the two silanes, DMDPS has two aromatic rings that give rise to ordered structures. Aromatic siloxanes induce a progressive decrease of the available surface area available for chemical reactivity and fill smaller “pores” present in a silane coating. This pore “clogging” by aromatic side chains, which are more rigid and more

organized than alkyl chains, are expected to produce increased hydrophobicity (Meroni et al., 2011). Comparison of condensation reactions show DMDPS involving two hydrolysable groups, whereas HMDS only has one hydrolysable group available for reaction. Consequently, each molecule of DMDPS removes twice as many OH^- groups during coating deposition. Differences in silane linkage length and size also play a role, as longer and larger linkages (i.e., R groups) impart greater hydrophobicity. DPMS, with its aromatic groups, has greater size and length than the methyl groups present in HDMS. Collectively, these factors are expected to impart greater hydrophobicity to DMDPS and thereby increase its contact angle with water.

Contact angle measurement with water on silica for HDMS has been reported to be 97 degrees (Grate et al., 2013). Contact angle measurement of DMDPS on silica is not available, but when adsorbed onto TiO_2 has been reported to be 133 degrees (Meroni et al. 2011). Different sources state superhydrophobicity occurs at contact angles greater than either 120 or 150 degrees (Arkles, 2006; Chang et al., 2009), which positions HDMS as hydrophobic (contact angle greater than 90 degrees) and DMDPS as generally superhydrophobic. Manufacturer description for KH220-coated silica states that the product is superlipophilic, and superlipophilic compounds also are often superhydrophobic. With these considerations, DMDPS can be considered to have superhydrophobic properties.

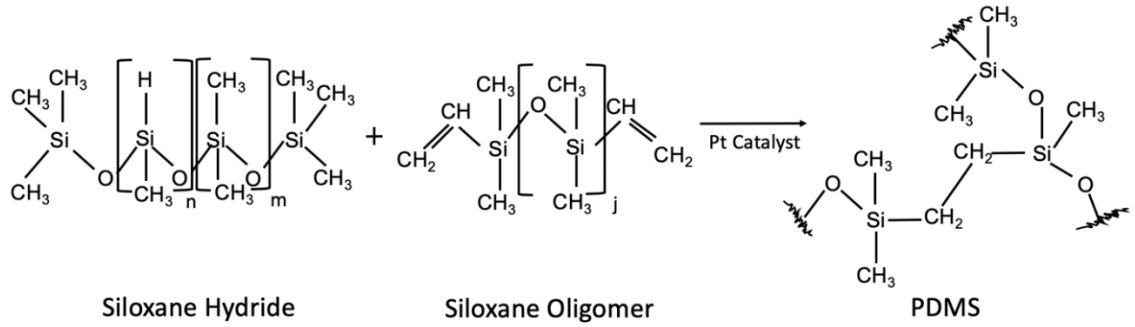

Figure 5.1 PDMS addition polymerization-crosslink formation of high temperature vulcanizing PDMS. n,m,j represent numbers of repeat units (Sturgess et al., 2017).

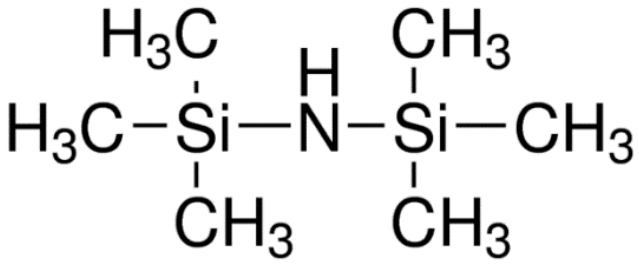

Figure 5.2 Hexamethyl disilazane present on submicron silica surface (TS530)

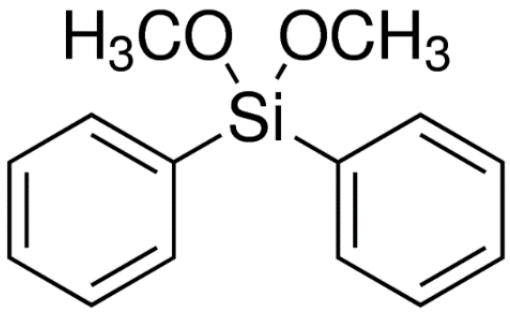

Figure 5.3 Dimethoxydiphenyl silane present on hydrophobic coated nanosilica surface (KH220)

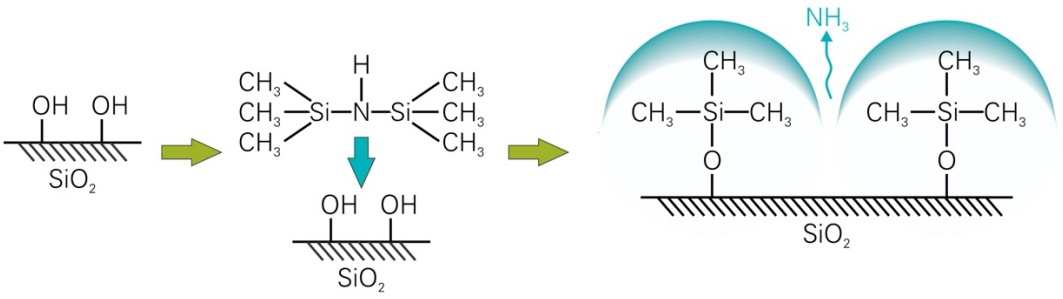

Figure 5.4 Chemical reactions for HMDS absorption onto silica. Hydrolysis results in formation of ammonia.

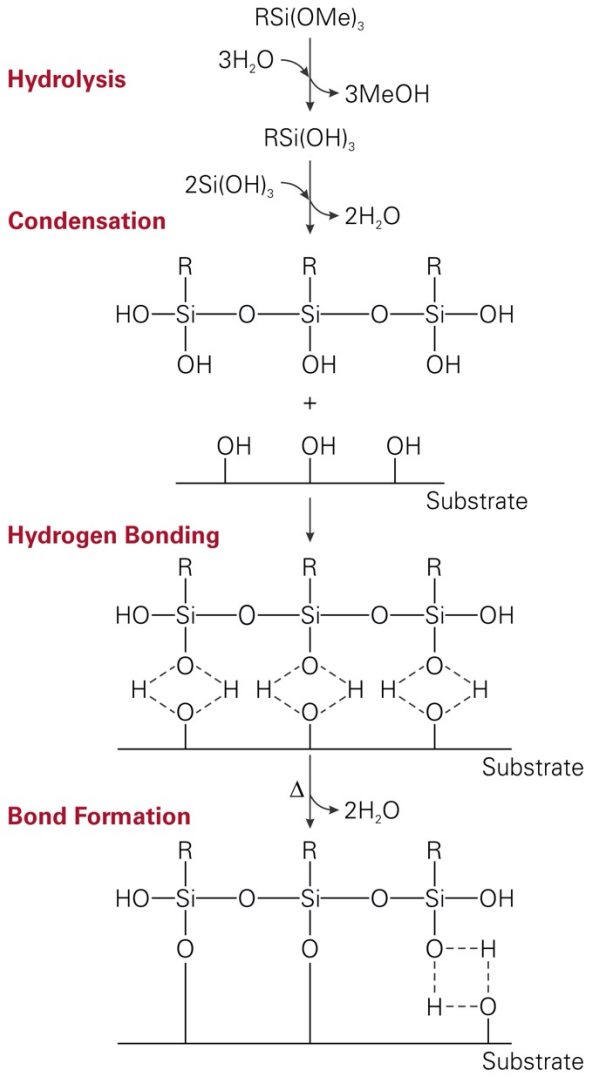

Figure 5.5 Chemical reactions for DMDPS absorption onto silica.

Submicron SiO_2-filled samples produced significantly greater failure strain compared to both nano-SiO_2 filled materials at all filler loadings. At 15% filler, failure strain was 1.4 – 1.6 times higher for submicron-filled siloxanes. Because elastomers undergo little, if any, plastic deformation prior to failure, failure strain changes inversely with the modulus. That is, stiffer materials undergo less strain at failure. An increased number of fillers and improved polymer adsorption by nanosized particles increase adhesion between particle-polymer and enhance polymer stiffness. This, in turn, restricts polymer chain movement and hence elongation at tensile failure. Similar observations have been reported when nanosilica are added to commercial silicone elastomers containing submicron particles. Additions above 1.5 weight percent decrease tensile failure strain. (Zayed et al., 2014).

Similar to tensile strength, superhydrophobic- coated nano-SiO_2-filled PDMS produced higher tear strength compared to uncoated nano-SiO_2- and submicron-filled PDMS. The tear strengths of coated nano-SiO_2 materials were approximately 1.2 times higher than two other filler types at 15% filler loading. Compared to unfilled PDMS materials, this represented a 640% increase. Tear strength represents resistance to crack propagation, and in composite materials, additional energy is needed to propagate a crack through a stiffer material, and/or grow a crack either around or through the particles. The excellent tear strength observed for coated nano-SiO_2-filled PDMS materials was attributed to strong adhesion between nanoparticles and polymer matrix, which effectively stiffened the materials and offered a physical barrier against growing cracks. (Mohammad et al., 2006). Crack growth is prevented by the rigid particles and hence, extra energy is required for crack propagation. Nanoparticles deviate the crack from its main plane, resulting in an increase in the surface area of the growing crack and the energy to propagate it (Ozdemir et al., 2016).

Similar findings have been reported by Zayed, et al. (2014), where the addition of 3% surface treated SiO_2 nanofiller to a commercial silicone produced significant improvements in tear strength compared to materials without nanoparticles. Chemical treatment of a silica filler with silane has been shown to improve filler incorporation into and reinforcement of the siloxane, resulting in increased material strength and tear resistance (Colas et al., 2004).

5.2 Durometer Hardness

Hardness is a surface phenomenon and is affected by the surface area of incorporated filler. In the Shore-A test, initial material resistance to indenter load is a combined elastic and viscous response, and hardness lowers over time as the material undergoes creep, which represents viscous deformation. According to ASTM Standard D2240, hardness is read on the dial gauge one second after the indenter contacts the elastomer surface. This permits an amount of viscous deformation to occur. The higher hardness values observed in nano-SiO2- filled polymers is attributed to the reinforcing behavior of nanoparticles, which increases stiffness and is expected to reduce the viscous response. Consequently, higher hardness is rendered, as shown in Figures 4.9 and 4.10.

Durometer hardness was not significantly affected by 3000 hours of outdoor weathering in both nano-SiO_2 filled groups. Meanwhile, after weathering, statistically significant hardness increases were observed in 10% and 15% submicron- filled polymers. Ultraviolet radiation degrades polymers through a radiolysis mechanism which enhances cross-linking and the production of smaller polymer chains that leads to volatile degradation products (Hatamleh et al., 2010; Cottin et al., 2000; Eleni et al., 2011). With ultraviolet radiation exposure being the primary cause of weathering-induced damage, the ability of fillers to block incident radiation is key to protecting the

surrounding polymer from chemical change. With as much as 10 times more nanoparticles present per unit volume, enhanced protection is offered over submicron particles, and chemical changes to the polymer are reduced. However, it should be acknowledged that the 2.6-unit maximum increase in Shore-A hardness observed by submicron-containing materials may not be clinically detectable when touching the surface of a facial prosthesis. This implies that clinically, these materials are equally adequate in maintaining hardness in the face of outdoor weathering. In previous studies, there were progressive hardenings of commercial prosthetic silicone elastomers after 9 months of outdoor weathering and hardening of a medical-grade PDMS after one-year outdoor weathering (Kheur et al., 2012; Eleni et al., 2011)). It is noteworthy that materials tested in these studies possessed submicron silica, which accounts for TS530-filled materials mirroring their results.

5.3 Translucency Parameter

Translucency is described as the ability of a material to permit background colors to affect the appearance of the material itself. Translucency parameter is determined by measuring reflected color on white and black backgrounds. A greater value for translucency parameter is indicative of greater translucency, or less opacity (Johnston et al., 1997). A material's translucency is dependent upon the combined effects of absorption and scattering. Light transmission through a material is affected by its composition, and for filled PDMS, both polymer matrix and fillers control the amount of light scattering and absorption. Filler volume fraction, filler size, and refractive indices of polymer and fillers affect light scattering and absorption (Son et al., 2016). In this study, both coated and uncoated nano-SiO_2- filled elastomers produced lower translucency parameter values than submicron SiO_2 – filled elastomers. Because nanoparticles provide large total surface area, they act to better block the reflectance off white and

black background to incident light. Therefore, their lower translucency parameters indicate greater masking abilities of underlying structures, which reduces the need for opacifiers added to a prosthesis (Johnston et al., 1995). This permits more accurate formulation of skin tones, as the whitening effect of opacifiers is reduced or eliminated.

For the two nanoparticle types, unfilled and lowly filled polymers (0%, 0.5%, 5%) experienced a five unit decrease in translucency parameter values after 3000 hours of outdoor weathering. This indicated the materials became more opaque. In visual observation, the samples darkened. Colorimetric changes demonstrated decreases of L* values (approximately 1 to 4 units) and increases of a* and b* values (approximately 0.1 to 2 units), which meant the materials primarily blackened and slightly turned more blue and red. Based on limits of perceptibility (1.3 units) and acceptability (4.4 units) in translucency parameter established by Paravina et al. (2019), the translucency changes (5 units) were not acceptable and would produce a mismatch in appearance between prosthesis and skin. This implies that a minimum of 10% nanofiller is needed to prevent these changes. These results are consistent with those reported by Tukmachi et al. (2017), where a significant decrease of light transmission through high-nanosilica-filled PDMS occurred, compared to lower percentages nanosilica. In dental resin composite, Lee et al. (2008) reported that composite filled with nanoparticles with higher filler content produced lower translucency parameter values.

5.4 Dynamic Mechanical Analysis (DMA)

DMA is a useful technique for experimental characterization of viscoelastic properties of polymers. DMA measures the dynamic modulus and viscoelastic damping under dynamic vibrational loading at different temperatures or frequencies. These properties change significantly when segmental mobility increases, and crystalline structures transition to the amorphous phase. Temperature dependence is best

identified when the test is conducted in stress-temperature mode, which was chosen for this study.

At -150^{o}C PDMS behaves as a glass, where polymer molecules are well anchored by hydrogen bonding and low thermal disturbance. This produces high values for storage modulus and low values for loss modulus, rendering the deformation response as elastic in nature. Temperature increases to Transition I decrease storage moduli and increase loss moduli for all formulations, including unfilled (Figs. 4.15 - 4.18). These moduli changes reflect a decrease in stiffness and increase in damping, which increases tan delta and appears as a spike on the graphs. At this temperature, the polymer is undergoing devitrification and reforming crystallites that were generated during cooling to -150^{o}C. A comparison of Transition I temperatures presented in Figs 4.15 – 4.18 and Table 4.15 demonstrate approximately 4 ^{o}C higher transition temperatures for 15%- filled formulations compared to unfilled PDMS. Since increasing temperatures are causing polymer chains to fold and align into crystallites, materials with more crystals require more thermal energy and hence higher temperatures. This also can be understood by viewing the reverse process, where materials with higher filler numbers more effectively nucleate crystals during cooling to -150^{o}C. Transition I temperatures occur earlier, at higher temperatures. Temperature transition trends appearing in table 4.15 also show for 5% and higher filled materials that KH220-filled PDMS consistently demonstrates higher transition temperatures than do uncoated- and TS530-filled PDMS. This is consistent with higher crystal numbers created by superhydrophobically coated particles promoting superior filler dispersion, where more nucleation sites are available.

A second tan delta peak is detected in curves for all samples at Transition II. During cooling from the melt, the PDMS molecules begin to undergo crystallization and form semi-crystalline polymers. Crystallites act as additional topological constrains and

reduce segmental mobility of polymer chains, and both storage and loss moduli increase as the polymer continues to cool. This can be seen as increases in slopes of moduli curves in Figs. 4.15 to 4.18. As crystallization proceeds with lowering temperatures, the polymer slowly stiffens. The presence of silica fillers provides nucleation sites for crystallization, thereby accelerating the crystallization process (Chien et al., 2006, Bosque et al., 2014). At Transition II, filler type and weight percent filler significantly affect transition temperatures. Temperatures presented in Table 4.17 demonstrate lower temperatures for 5% and 10% TS530-filled PDMS compared to coated- and uncoated-nano-filled PDMS. Because filler presence promotes crystallization, more fillers equate to more crystals and higher crystallization rates. With ten times more particles present in nanofilled formulations, crystallization occurs sooner during cooling and hence produces higher Transition II temperatures.

At transition III, a high spike of tan delta occurs, as shown in Figs. 4.15, 4.17 and 4.18, indicating viscous behavior dramatically increases, thereby raising E”/E’ ratio. Transition III corresponds to melt temperature during heating and solidification during cooling. For elastomers, in-service stretchability at ambient temperature is referenced as the melt condition. At this temperature, a partially crystalline solid is converted to a rubbery one during heating through “melting” of the crystallites, causing remarkable damping to occur. Careful inspection of Figs. 4.15, 4.17, and 4.18 reveal an increase in storage modulus that producers a small “hump” in the curve at temperatures below the melt temperature. During cooling, the loss of rubbery behavior occurred through the start of crystal formation. Consequently, polymer stiffening occurred and produced the hump. For uncoated and TS530-filled materials, Transition III produces trends similar to those observed for Transitions I and II, where increasing filler content tends to drive the transition temperature upward (Table 4.19). However, KH220-filled materials show erratic raising and lowering of temperature when filler increases, which are

unexplainable. Regardless of temperature differences, mechanical properties are unaffected, as storage and loss moduli are similar for all materials at all filler loadings at the Transition III temperature (Table 4.11).

As temperatures increase into the plateau region during heating, storage moduli values for all formulations decrease approximately ten-fold as 20^{o}C is approached. Significant differences presented in Table 4.13 demonstrate higher storage moduli values occur as filler levels increase for the three filler types, with highest storage moduli present for nanosilica-filled formulations, for reasons previously discussed. Decreases in loss moduli over this temperature range are more dramatic, as 100-fold decreases place loss moduli values in the 1 – 20 kPa range. Overall, this produces the highly elastic material response characteristic of elastomers at ambient temperatures.

5.5 Conclusions

The purpose of this research was to study PDMS filled with uncoated and hydrophobic-coated nano-SiO_2 and compare their mechanical behaviors with those measured for a conventional submicron-filled PDMS.

Conclusions of this study are as follows:

1. PDMS elastomers loaded with 15% superhydrophobic coated nano-SiO_2 produced the highest tensile strength, elastic modulus, tear strength and durometer hardness.
2. PDMS elastomers filled with 15% submicron SiO_2 produced the highest failure strain and translucency parameter values.
3. Durometer hardness was not affected by 3000 hours outdoor weathering in all groups, except for 10%- and 15%- filled submicron SiO_2 elastomers, which hardened by 2.6 hardness units.

4. Unfilled and 0.5% filled elastomer experienced decreases of translucency parameter values after 3000 hours of outdoor weathering, while higher filled loading materials maintained their translucency parameter values.
5. Transition temperatures of filled PDMS were higher than those for unfilled PDMS.

5.6 Clinical/Translational Implications

Successful engineering of facial prosthetic materials to cover facial defects while also providing a skin-like feel is expected to require multiple materials stacked together, where reinforcing base materials are covered with a compressible surface layer. This can be realized through additive manufacturing, where a gradient of physical properties is achieved with different materials deposited via a three-dimensional printing process. Elastomers studied in this project provided fundamental knowledge regarding the effects that compositional differences rendered on key physical properties. The intent was to better understand the role played by filler loadings, coatings, and sizes for development of a skin-like material to be applied as surface layer. Results presented here demonstrated that silica nanoparticles with a high degree of hydrophobicity must be considered for inclusion within a PDMS polymer in order to provide adequate strength, tear resistance and masking ability, but the filler levels must be controlled to approximately ten weight percent to retain adequate compressibility.

5.7 Limitations

Limitations associated with this project include the following:

1. Although Durometer hardness was used to assess consistency among different mixed batches of filled-PDMS, small batch-to-batch differences were expected.
2. Tensile and tear properties affected by outdoor weathering could not be studied due to a limitation of raw materials.

3. Standard material property tests that simulate the touch and feel of human skin are not available, which prohibit direct comparisons.
4. Outdoor weathering exposures cannot be duplicated, and accelerated tests do not impart the same exposures as those expected for normal prosthesis wear. Therefore outdoor weathering tests must be viewed as estimates of actual material behaviour.

5.8 Future Research

Future research on this topic should include examination of tensile and tear property changes generated by outdoor weathering exposure. This will provide a more in-depth understanding about potential underlying mechanisms behind physical property changes in nano filled PDMS materials.

Based on the results of this study, future research should assess physical properties of materials filled with a combination of nanoparticles and submicron particles. This may optimize different properties and better achieve desirable skin-like properties.

Technology is being developed for sensing touch by disabled patients requiring prosthetic rehabilitation. Future research should explore adapting these technologies to develop both laboratory and clinical instruments that will provide direct assessment of material reproducibility of skin at different facial locations.

Bibliography

Allaker, R. P., & Ren, G. (2008). Potential impact of nanotechnology on the control of infectious diseases. *Transactions of the Royal Society of Tropical Medicine and Hygiene, 102*(1), 1-2. doi:S0035-9203(07)00233-7 [pii]

Andres, C. J., & Haug, S. P. (2000). Facial prosthesis fabrication: coloration techniques. *Clinical maxillofacial prosthetics. Quintessence Publishing Co, Inc*, 233-44.

Andres, C. J., Haug, S. P., Munoz, C. A., & Bernal, G. (1992). Effects of environmental factors on maxillofacial elastomers: Part I--literature review. *Journal of Prosthetic Dentistry, 68*(2), 327-330. doi:0022-3913(92)90339-C [pii]

Arkles, B. (2006). Hydrophobicity, hydrophilicity and silanes. *Paint & Coatings Industry Magazine*, *22*(12), 114-135.

ASTM D2240 (2005), Standard Test Method for Rubber Property—Durometer Hardness, ASTM International, West Conshohocken, PA, 2005, www.astm.org

ASTM D412 (2002), Standard Test Methods for Vulcanized Rubber and Thermoplastic Elastomers—Tension, ASTM International, West Conshohocken, PA, 2002, www.astm.org

ASTM D624 (2001), Standard Test Method for Tear Strength of Conventional Vulcanized Rubber and Thermoplastic Elastomers, ASTM International, West Conshohocken, PA, 2001, www.astm.org

Aziz, T., Waters, M., & Jagger, R. (2003a). Analysis of the properties of silicone rubber maxillofacial prosthetic materials. *Journal of Dentistry, 31*(1), 67-74. doi:S0300571202000842 [pii]

Aziz, T., Waters, M., & Jagger, R. (2003b). Development of a new poly(dimethylsiloxane) maxillofacial prosthetic material. *Journal of Biomedical Materials Research.Part B, Applied Biomaterials, 65*(2), 252-261. doi:10.1002/jbm.b.10559 [doi]

Balos, S., Pilic, B., Markovic, D., Pavlicevic, J., & Luzanin, O. (2014). Poly(methyl-methacrylate) nanocomposites with low silica addition. *Journal of Prosthetic Dentistry, 111*(4), 327-334. doi:10.1016/j.prosdent.2013.06.021 [doi]

Bangera, B. S., & Guttal, S. S. (2014). Evaluation of varying concentrations of nano-oxides as ultraviolet protective agents when incorporated in maxillofacial silicones: An in vitro study. *Journal of Prosthetic Dentistry, 112*(6), 1567-1572. doi:10.1016/j.prosdent.2014.07.001 [doi]

Barnhart, G. W. (1960). Silicone rubber as a resilient denture base material. *Journal of Dental Research, 39*, 1077. doi:10.1177/00220345600390051801 [doi]

Beatty, M. W., Mahanna, G. K., & Jia, W. (1999). Ultraviolet radiation-induced color shifts occurring in oil-pigmented maxillofacial elastomers. *Journal of Prosthetic Dentistry,* 82(4), 441-446. doi:https://doi.org/10.1016/S0022-3913(99)70031-4

Beatty, M. W., Mahanna, G. K., Dick, K., & Jia, W. (1995). Color changes in dry-pigmented maxillofacial elastomer resulting from ultraviolet light exposure. *Journal of Prosthetic Dentistry,* 74(5), 493-498. doi:https://doi.org/10.1016/S0022-3913(05)80351-8

Beatty, M. W., Swartz, M. L., Moore, B. K., Phillips, R. W., & Roberts, T. A. (1998). Effect of microfiller fraction and silane treatment on resin composite properties. *Journal of Biomedical Materials Research, 40*(1), 12-23. doi:10.1002/(SICI)1097-4636(199804)40:1<12::AID-JBM2>3.0.CO;2-U [pii]

Bellamy, K., Limbert, G., Waters, M. G., & Middleton, J. (2003). An elastomeric material for facial prostheses: Synthesis, experimental and numerical testing aspects. *Biomaterials.* 24(27), 5061-5066. doi:https://doi.org/10.1016/S0142-9612(03)00412-5

Belyakova, L. A., & Varvarin, A. M. (1999). Surfaces properties of silica gels modified with hydrophobic groups. *Colloids and Surfaces A: Physicochemical and Engineering Aspects*, *154*(3), 285-294.

Bosq, N., Guigo, N., Persello, J., & Sbirrazzuoli, N. (2014). Melt and glass crystallization of PDMS and PDMS silica nanocomposites. *Physical Chemistry Chemical Physics*, *16*(17), 7830-7840.

Brandao, T. B., Vechiato Filho, A. J., de Souza Batista, V. E., Prado Ribeiro, A. C., Filho, H. N., Chilvarquer, I., Wee, A. G. (2017). Assessment of treatment outcomes for facial prostheses in patients with craniofacial defects: A pilot retrospective study. *Journal of Prosthetic Dentistry, 118*(2), 235-241. doi:S0022-3913(16)30578-9 [pii]

Breitbart, W., & Holland, J. (1988). Psychosocial aspects of head and neck cancer. *Seminars in Oncology, 15*(1), 61-69.

Camenzind, A., Schweizer, T., Sztucki, M., & Pratsinis, S. E. (2010). Structure & strength of silica-PDMS nanocomposites. *Polymer.* 51(8), 1796-1804. doi:https://doi.org/10.1016/j.polymer.2010.02.030

Cantor, R., Webber, R. L., Stroud, L., & Ryge, G. (1969). Methods for evaluating prosthetic facial materials. *Journal of Prosthetic Dentistry.* 21(3), 324-332. doi:https://doi.org/10.1016/0022-3913(69)90295-9 "

Cevik, P., & Eraslan, O. (2017). Effects of the addition of titanium dioxide and silaned silica nanoparticles on the mechanical properties of maxillofacial silicones. *Journal of Prosthodontics, 26*(7), 611-615. doi:10.1111/jopr.12438 [doi]

Chalian, V. A., & Phillips, R. W. (1974). Materials in maxillofacial prosthetics. *Journal of Biomedical Materials Research, 8*(4 Pt 2), 349-363. doi:10.1002/jbm.820080415 [doi]

Champion, H. R., Holcomb, J. B., Lawnick, M. M., Kelliher, T., Spott, M. A., Galarneau, M. R., Shair, E. K. (2010). Improved characterization of combat injury. *Journal of Trauma, 68*(5), 1139-1150. doi:10.1097/TA.0b013e3181d86a0d [doi]

Chang, F. M., Hong, S. J., Sheng, Y. J., & Tsao, H. K. (2009). High contact angle hysteresis of superhydrophobic surfaces: hydrophobic defects. *Applied physics letters*, *95*(6), 064102.

Chang, T. L., Garrett, N., Roumanas, E., & Beumer, J.,3rd. (2005). Treatment satisfaction with facial prostheses. *Journal of Prosthetic Dentistry, 94*(3), 275-280. doi:S0022-3913(05)00317-3 [pii]

Chen, M. S., Udagama, A., & Drane, J. B. (1981). Evaluation of facial prostheses for head and neck cancer patients. *Journal of Prosthetic Dentistry, 46*(5), 538-544. doi:0022-3913(81)90244-4 [pii]

Chien, A., Maxwell, R. S., DeTeresa, S., Thompson, L., Cohenour, R., & Balazs, B. (2006). Effects of filler–polymer interactions on cold-crystallization kinetics in crosslinked, silica-filled polydimethylsiloxane/polydiphenylsiloxane copolymer melts. *Journal of Polymer Science Part B: Polymer Physics*, *44*(13), 1898-1906.

Chieruzzi, M., Pagano, S., Moretti, S., Pinna, R., Milia, E., Torre, L., & Eramo, S. (2016). Nanomaterials for tissue engineering in dentistry. *Nanomaterials (Basel, Switzerland), 6*(7), 10.3390/nano6070134. doi:E134 [pii]

Chiulan, I., Panaitescu, D. M., Radu, E. R., Frone, A. N., Gabor, R. A., Nicolae, C. A., Chinga-Carrasco, G. (2020). Comprehensive characterization of silica-modified silicon rubbers. *Journal of the Mechanical Behavior of Biomedical Materials, 101*, 103427. doi:S1751-6161(19)30614-9 [pii]

Choi, S. S., Nah, C., Lee, S. G., & Joo, C. W. (2003). Effect of filler–filler interaction on rheological behaviour of natural rubber compounds filled with both carbon black and silica. *Polymer International*, *52*(1), 23-28.

Clarke, A. (1999). Psychosocial aspects of facial disfigurement: Problems, management and the role of a lay-led organization. Psychology, Health and Medicine, 4, 127–142.

Colas, A. and Curtis, J. (2004). Silicone Biomaterials: History and Chemistry. Biomaterials Science, 2nd Ed. *An Introduction to Materials in Medicine,* Academic Press: 80-86.

Cottin, H., Gazeau, M., Doussin, J., & Raulin, F. (2000). An experimental study of the photodegradation of polyoxymethylene at 122, 147 and 193 nm. *Journal of Photochemistry and Photobiology A: Chemisty,* 135(1), 53-64. doi:https://doi.org/10.1016/S1010-6030(00)00274-4

Craig, R. G., Koran, A., Yu, R., & Spencer, J. (1978). Color stability of elastomers for maxillofacial appliances. *Journal of Dental Research, 57*(9-10), 866-871. doi:10.1177/00220345780570090401 [doi]

De Sousa, A. (2010). Psychological issues in acquired facial trauma. *Indian Journal of Plastic Surgery, 43*(2), 200-205. doi:10.4103/0970-0358.73452 [doi]

dos Santos, D. M., Goiato, M. C., Moreno, A., Pesqueira, A. A., & Haddad, M. F. (2011). Influence of pigments and opacifiers on color stability of an artificially aged facial silicone. *Journal of Prosthodontics, 20*(3), 205-208. doi:10.1111/j.1532-849X.2010.00657.x [doi]

dos Santos, D. M., Goiato, M. C., Sinhoreti, M. A., Fernandes, A. U., Ribeiro Pdo, P., & Dekon, S. F. (2010). Color stability of polymers for facial prosthesis. *Journal of Craniofacial Surgery, 21*(1), 54-58. doi:10.1097/SCS.0b013e3181c3b58e [doi]

Duevel, D., Beatty, M., & Simetich, B. (2015). Coated nanoparticles and polymer molecular weight- effects on PDMS properties. *Journal of Dental Research,* 94(Special Issue A), 3568 [Abstract].

Eggbeer, D., Evans, P. L., & Bibb, R. (2006). A pilot study in the application of texture relief for digitally designed facial prostheses. *Proceedings of the Institution of Mechanical Engineers.Part H, Journal of Engineering in Medicine, 220*(6), 705-714. doi:10.1243/09544119JEIM38 [doi]

El-Kady, O., & Fathy, A. (2014). Effect of SiC particle size on the physical and mechanical properties of extruded al matrix nanocomposites. *Materials and Design.* 54, 348-353. doi:https://doi.org/10.1016/j.matdes.2013.08.049

Eleni, P. N., Katsavou, I., Krokida, M. K., Polyzois, G. L., & Gettleman, L. (2009). Mechanical behavior of facial prosthetic elastomers after outdoor weathering. *Dental Materials, 25*(12), 1493-1502. doi:10.1016/j.dental.2009.06.018 [doi]

Eleni, P. N., Krokida, M., Polyzois, G., Gettleman, L., & Bisharat, G. I. (2011). Effects of outdoor weathering on facial prosthetic elastomers. *Odontology, 99*(1), 68-76. doi:10.1007/s10266-010-0145-0 [doi]

Fragiadakis, D., Pissis, P., & Bokobza, L. (2005). Glass transition and molecular dynamics in poly(dimethylsiloxane)/silica nanocomposites. *Polymer,* 46(16), 6001-6008. doi:https://doi.org/10.1016/j.polymer.2005.05.080

Fu, S., Feng, X., Lauke, B., & Mai, Y. (2008). Effects of particle size, particle/matrix interface adhesion and particle loading on mechanical properties of particulate–polymer composites. *Composites Part B: Engineering,* 39(6), 933-961. doi:https://doi.org/10.1016/j.compositesb.2008.01.002

Goiato, M. C., Haddad, M. F., Sinhoreti, M. A., dos Santos, D. M., Pesqueira, A. A., & Moreno, A. (2010). Influence of opacifiers on dimensional stability and detail reproduction of maxillofacial silicone elastomer. *Biomedical Engineering Online, 9*, 85-85. doi:10.1186/1475-925X-9-85 [doi]

Goiato, M. C., Pesqueira, A. A., Ramos da Silva, C., Gennari Filho, H., & Micheline Dos Santos, D. (2009). Patient satisfaction with maxillofacial prosthesis. literature review. *Journal of Plastic, Reconstructive & Aesthetic Surgery : JPRAS, 62*(2), 175-180. doi:10.1016/j.bjps.2008.06.084 [doi]

Goiato, M. C., Pesqueira, A. A., Santos, D. M., & Dekon, S. F. (2009). Evaluation of hardness and surface roughness of two maxillofacial silicones following disinfection. *Brazilian Oral Research, 23*(1), 49-53. doi:S1806-83242009000100009 [pii]

Gun'Ko, V. M., Vedamuthu, M. S., Henderson, G. L., & Blitz, J. P. (2000). Mechanism and kinetics of hexamethyldisilazane reaction with a fumed silica surface. *Journal of colloid and interface science*, *228*(1), 157-170.

Gupta, A., Jain, D., Tripathi, K., & Bhujle, A. G. (2009). Dynamic visco-elastic analysis of silicone maxillo-facial prosthetic material using custom-made dynamic visco-elastometer and LASER measuring device. *The Journal of Indian Prosthodontic Society*, *9*(3), 127.

Han, Y., Kiat-amnuay, S., Powers, J. M., & Zhao, Y. (2008). Effect of nano-oxide concentration on the mechanical properties of a maxillofacial silicone elastomer. *Journal of Prosthetic Dentistry, 100*(6), 465-473. doi:10.1016/S0022-3913(08)60266-8 [doi]

Hatamleh, M. M., & Watts, D. C. (2010). Mechanical properties and bonding of maxillofacial silicone elastomers. *Dental Materials, 26*(2), 185-191. doi:10.1016/j.dental.2009.10.001 [doi]

Hatamleh, M. M., Polyzois, G. L., Nuseir, A., Hatamleh, K., & Alnazzawi, A. (2016). Mechanical properties and simulated aging of silicone maxillofacial elastomers: Advancements in the past 45 years. *Journal of Prosthodontics, 25*(5), 418-426. doi:10.1111/jopr.12409 [doi]

Haug, S. P., Moore, B. K., & Andres, C. J. (1999). Color stability and colorant effect on maxillofacial elastomers. part II: Weathering effect on physical properties. *Journal of Prosthetic Dentistry, 81*(4), 423-430. doi:S002239139900089X [pii]

Head and Neck Cancer. (2017). Head and neck cancer statistic. Retrieved from https://www.cancer.net/cancer-types/head-and-neck-cancer/statistics

Heilbronn, C. M., Svider, P. F., Folbe, A. J., Shkoukani, M. A., Carron, M. A., Eloy, J. A., & Zuliani, G. (2015). Burns in the head and neck: A national representative analysis of emergency department visits. *The Laryngoscope, 125*(7), 1573-1578. doi:10.1002/lary.25132 [doi]

Hirasawa, T. (1963). Studies on the self-curing resin containing inorganic filler for dental restoration (I) on the mechanical properties.*Tokyo Med Dent Univ Res Inst Dent Mater, 2*(5), 443-456. Retrieved from https://ci.nii.ac.jp/naid/10005690166/en/

Hu, X., & Johnston, W. M. (2011). Translucency estimation for thick pigmented maxillofacial elastomer. *Journal of Dentistry,* 39(1), 2-8. doi:https://doi.org/10.1016/j.jdent.2011.01.002

Jani, R. M., & Schaaf, N. G. (1978). An evaluation of facial prostheses. *Journal of Prosthetic Dentistry, 39*(5), 546-550. doi:S0022-3913(78)80191-7 [pii]

Johnston, W. M., Ma, T., & Kienle, B. H. (1995). Translucency parameter of colorants for maxillofacial prostheses. *The International Journal of Prosthodontics, 8*(1), 79-86.

Klonos, P., Panagopoulou, A., Bokobza, L., Kyritsis, A., Peoglos, V., & Pissis, P. (2010). Comparative studies on effects of silica and titania nanoparticles on crystallization and complex segmental dynamics in poly(dimethylsiloxane*). Polymer,* 51(23), 5490-5499. doi:https://doi.org/10.1016/j.polymer.2010.09.054

Koran, A., & Craig, R. G. (1975). Dynamic mechanical properties of maxillofacial materials. *Journal of Dental Research, 54*(6), 1216-1221. doi:10.1177/00220345750540062001 [doi]

Koran, A., Yu, R., Powers, J. M., & Craig, R. G. (1979). Color stability of a pigmented elastomer for maxillofacial appliances. *Journal of Dental Research, 58*(5), 1450-1454. doi:10.1177/00220345790580050301 [doi]

Lai, J. H., Wang, L. L., Ko, C. C., DeLong, R. L., & Hodges, J. S. (2002). New organosilicon maxillofacial prosthetic materials. *Dental Materials, 18*(3), 281-286. doi:S0109564101000501 [pii]

Lampman, S. (2003). *Characterization and failure analysis of plastics*. ASM International.

Lee, Y. (2008). Influence of filler on the difference between the transmitted and reflected colors of experimental resin composites. *Dental Materials,* 24(9), 1243-1247. doi:https://doi.org/10.1016/j.dental.2008.01.014

Lemon, J. C., Kiat-amnuay, S., Gettleman, L., Martin, J. W., & Chambers, M. S. (2005). Facial prosthetic rehabilitation: Preprosthetic surgical techniques and biomaterials. *Current Opinion in Otolaryngology & Head and Neck Surgery, 13*(4), 255-262. doi:00020840-200508000-00010 [pii]

Levine, E., Degutis, L., Pruzinsky, T., Shin, J., & Persing, J. A. (2005). Quality of life and facial trauma: Psychological and body image effects. *Annals of Plastic Surgery, 54*(5), 502-510. doi:00000637-200505000-00010 [pii]

Lew, T. A., Walker, J. A., Wenke, J. C., Blackbourne, L. H., & Hale, R. G. (2010). Characterization of craniomaxillofacial battle injuries sustained by united states service members in the current conflicts of iraq and afghanistan. *Journal of Oral and Maxillofacial Surgery, 68*(1), 3-7. doi:10.1016/j.joms.2009.06.006 [doi]

Lewis, D. H., & Castleberry, D. J. (1980). An assessment of recent advances in external maxillofacial materials. *Journal of Prosthetic Dentistry, 43*(4), 426-432. doi:0022-3913(80)90215-2 [pii]

Liu, J., Wu, S., Zou, M., Zheng, X., & Cai, Z. (2012). Surface modification of silica and its compounding with polydimethylsiloxane matrix: interaction of modified silica filler with PDMS. *Iranian Polymer Journal*, *21*(9), 583-589. Ltd.

Lynch, W. (1978). *Handbook of silicone rubber fabrication*. Van Nostrand Reinhold Company.

Mahajan, H., & Gupta, S. K. (2012). Maxillofacial prosthetic materials: A literature review. *Journal of Orofacial Research, 2*(2), 87-90.

Mahomed, A., Chidi, N. M., Hukins, D. W., Kukureka, S. N., & Shepherd, D. E. (2009). Frequency dependence of viscoelastic properties of medical grade silicones. *Journal of Biomedical Materials Research.Part B, Applied Biomaterials, 89*(1), 210-216. doi:10.1002/jbm.b.31208 [doi]

Meroni, D., Ardizzone, S., Cappelletti, G., Ceotto, M., Ratti, M., Annunziata, R., Raimondi, L. (2011). Interplay between chemistry and texture in hydrophobic TiO2 hybrids. *Journal of Physical Chemistry C*, *115*(38), 18649-18658.

Meyers, K. O., Bye, M. L., & Merrill, E. W. (1980). Model Silicone Elastomer Networks of High Junction Functionality: Synthesis, Tensile Behavior, Swelling Behavior, and Comparison with Molecular Theories of Rubber Elasticity. *Macromolecules*, *13*(5), 1045-1053.

Mohammad, A., & Simon, G. P. (2006). In Mai Y., Yu Z.(Eds.), *12 - rubber-clay nanocomposites* Woodhead Publishing. doi:https://doi.org/10.1533/9781845691127.1.297

Mohammed, M., Tatineni, J., Cadd, B., Peart, P., & Gibson, I. (2016). Applications of 3D topography scanning and multi-material additive manufacturing for facial prosthesis development and production. In *Proceedings of the 27th Annual International Solid Freeform Fabrication Symposium* (pp. 1695-1707).

Mouzakis, D. E., Papadopoulos, T. D., Polyzois, G. L., & Griniari, P. G. (2010). Dynamic mechanical properties of a maxillofacial silicone elastomer incorporating a ZnO additive: the effect of artificial aging. *Journal of Craniofacial Surgery*, *21*(6), 1867-1871.

Murata, H., Hong, G., Hamada, T., & Polyzois, G. L. (2003). Dynamic mechanical properties of silicone maxillofacial prosthetic materials and the influence of frequency and temperature on their properties. *The International Journal of Prosthodontics, 16*(4), 369-374.

Nguyen, C. T., Chambers, M. S., Powers, J. M., & Kiat-Amnuay, S. (2013). Effect of opacifiers and UV absorbers on pigmented maxillofacial silicone elastomer, part 2: Mechanical properties after artificial aging. *Journal of Prosthetic Dentistry, 109*(6), 402-410. doi:10.1016/S0022-3913(13)60328-5 [doi]

Nie, Y., Gu, Z., Wei, Y., Hao, T., & Zhou, Z. (2017). Features of strain-induced crystallization of natural rubber revealed by experiments and simulations. *Polymer Journal*, *49*(3), 309-317.

Nobrega, A. S., Andreotti, A. M., Moreno, A., Sinhoreti, M. A., Dos Santos, D. M., & Goiato, M. C. (2016). Influence of adding nanoparticles on the hardness, tear strength, and permanent deformation of facial silicone subjected to accelerated aging. *Journal of Prosthetic Dentistry, 116*(4), 623-629.e1. doi:S0022-3913(16)30001-4 [pii]

Nobrega, L. M., Cavalcante, G. M., Lima, M. M., Madruga, R. C., Ramos-Jorge, M. L., & d'Avila, S. (2014). Prevalence of facial trauma and associated factors in victims of road traffic accidents. *The American Journal of Emergency Medicine, 32*(11), 1382-1386. doi:10.1016/j.ajem.2014.08.054 [doi]

Nogueira, T. E., Adorno, M., Mendonca, E., & Leles, C. (2018). Factors associated with the quality of life of subjects with facial disfigurement due to surgical treatment of head and neck cancer. *Medicina Oral, Patologia Oral Y Cirugia Bucal, 23*(2), e132-e137. doi:10.4317/medoral.22072 [doi]

Owens, B. D., Kragh, J. F.,Jr, Wenke, J. C., Macaitis, J., Wade, C. E., & Holcomb, J. B. (2008). Combat wounds in operation iraqi freedom and operation enduring freedom. *Journal of Trauma, 64*(2), 295-299. doi:10.1097/TA.0b013e318163b875 [doi]

Ozdemir, N. G., Zhang, T., Aspin, I., Scarpa, F., Hadavinia, H., & Song, Y. (2016). Toughening of carbon fibre reinforced polymer composites with rubber nanoparticles for advanced industrial applications. *Express Polymer Letters*, *10*(5).

Palousek, D., Rosicky, J., & Koutny, D. (2014). Use of digital technologies for nasal prosthesis manufacturing. *Prosthetics and Orthotics International, 38*(2), 171-175. doi:10.1177/0309364613489333 [doi]

Paravina, R. D., Perez, M. M., & Ghinea, R. (2019). Acceptability and perceptibility thresholds in dentistry: A comprehensive review of clinical and research applications. *Journal of Esthetic and Restorative, 31*(2), 103-112. doi:10.1111/jerd.12465 [doi]

Petrovic, Z., Javni, I., Waddon, A., & Banhegyi, G. (1999). Structure and properties of Polyurethane–Silica nanocomposites.*Journal of Applied Polymer Science Vol. 76*, 133–151 (2000).

Polyzois, G. L. (1999). Color stability of facial silicone prosthetic polymers after outdoor weathering*. Journal of Prosthetic Dentistry,* 82(4), 447-450. doi:https://doi.org/10.1016/S0022-3913(99)70032-6

Polyzois, G. L., Eleni, P. N., & Krokida, M. K. (2011). Optical properties of pigmented polydimethylsiloxane prosthetic elastomers: Effect of "outdoor" and "indoor" accelerating aging. *Journal of Craniofacial Surgery, 22*(5), 1574-1578. doi:10.1097/SCS.0b013e31822e5ca4 [doi]

Pratt, H., Hassanin, K., Troughton, L. D., Czanner, G., Zheng, Y., McCormick, A. G., & Hamill, K. J. (2017). UV imaging reveals facial areas that are prone to skin cancer are disproportionately missed during sunscreen application. *PLoS One*, *12*(10), e0185297.

Rahman, I. A., & Padavettan, V. (2012). Synthesis of silica nanoparticles by sol-gel: size-dependent properties, surface modification, and applications in silica-polymer nanocomposites—a review. *Journal of Nanomaterials*, *2012*.

Ramanathan, T., Stankovich, S., Dikin, D. A., Liu, H., Shen, H., Nguyen, S. T., & Brinson, L. C. (2007). Graphitic nanofillers in PMMA nanocomposites—an investigation of particle size and dispersion and their influence on nanocomposite properties. *Journal of Polymer Science Part B: Polymer Physics*, *45*(15), 2097-2112.

Ray, S., & Bhowmick, A. K. (2004). Influence of untreated and novel electron beam modified surface coated silica filler on dynamic mechanical thermal properties of ethylene-octene copolymer. *Polymer Engineering & Science*, *44*(1), 163-178.

Rothon R (Ed.) (2003). *Particulate-filled polymer composites*. iSmithers Rapra Publishing. Shrewsbury, UK, 489-490.

Santawisuk, W., Kanchanavasita, W., Sirisinha, C., & Harnirattisai, C. (2010). Dynamic viscoelastic properties of experimental silicone soft lining materials. *Dental Materials Journal, 29*(4), 454-460. doi:JST.JSTAGE/dmj/2009-126 [pii]

Schmalz, G., Hickel, R., van Landuyt, K. L., & Reichl, F. (2017). Nanoparticles in dentistry.*Dental Materials,33(11), 1298-1314.* doi:https://doi.org/10.1016/j.dental.2017.08.193

Shrivastava, A. (2018). In Shrivastava A. (Ed.), *Plastic properties and testing* William Andrew Publishing. doi:https://doi.org/10.1016/B978-0-323-39500-7.00003-4

Son, S. A., Park, J. K., Seo, D. G., Ko, C. C., & Kwon, Y. H. (2017). How light attenuation and filler content affect the microhardness and polymerization shrinkage and translucency of bulk-fill composites? *Clinical Oral Investigations, 21*(2), 559-565. doi:10.1007/s00784-016-1920-2 [doi]

St Germain, H., Swartz, M. L., Phillips, R. W., Moore, B. K., & Roberts, T. A. (1985). Properties of microfilled composite resins as influenced by filler content. *Journal of Dental Research, 64*(2), 155-160. doi:10.1177/00220345850640021301 [doi]

Stathi, K., Tarantili, P. A., & Polyzois, G. (2010). The effect of accelerated ageing on performance properties of addition type silicone biomaterials. *Journal of Materials Science.Materials in Medicine, 21*(5), 1403-1411. doi:10.1007/s10856-010-3991-y [doi]

Sturgess, C., Tuck, C. J., Ashcroft, I. A., & Wildman, R. D. (2017). 3D reactive inkjet printing of polydimethylsiloxane. *Journal of Materials Chemistry C*, *5*(37), 9733-9743.

Sweeney, W. T., Fischer, T. E., Castleberry, D. J., & Cowperthwaite, G. F. (1972). Evaluation of improved maxillofacial prosthetic materials. *Journal of Prosthetic Dentistry - 0376364, 27*(3), 297-305. doi:0022-3913(72)90039-X [pii]

Tanahashi, M., Hirose, M., Lee, J. C., & Takeda, K. (2006). Organic/inorganic nanocomposites prepared by mechanical smashing of agglomerated silica ultrafine particles in molten thermoplastic resin. *Polymers for advanced technologies*, *17*(11-12), 981-990.

Tang E, Cheng G, Pang X (2006). Synthesis of nano ZnO/poly(methylmethacrylate) composite microsphere through emulsion polymerization and its UV-shielding property. *Colloid and Polymer Science* 284(4):422-428.

Tetteh, S., Bibb, R. J., & Martin, S. J. (2017). Maxillofacial prostheses challenges in resource constrained regions. *Disability and Rehabilitation,* , 1-9. doi:10.1080/09638288.2017.1390697 [doi]

Thiele, O. C., Brom, J., Dunsche, A., Ehrenfeld, M., Federspil, P., Frerich, B., Zoller, J. E. (2015). The current state of facial prosthetics - A multicenter analysis. *Journal of Cranio-Maxillo-Facial Surgery, 43*(7), 1038-1041. doi:10.1016/j.jcms.2015.04.024 [doi]

Thomas, K. (1994). *Prosthetic Rehabilitation*. London, Quintessence Publishing

Tukmachi, M., & Moudhaffer, M. (2017). Effect of nano silicon dioxide addition on some properties of heat vulcanized maxillofacial silicone elastomer. *IOSR-JPBS*, *12*(3), 37-43.

van Schooneveld, M. M., Vucic, E., Koole, R., Zhou, Y., Stocks, J., Cormode, D. P., Mulder, W. J. (2008). Improved biocompatibility and pharmacokinetics of silica nanoparticles by means of a lipid coating: A multimodality investigation. *Nano Letters, 8*(8), 2517-2525. doi:10.1021/nl801596a [doi]

Wang, L., Liu, Q., Jing, D., Zhou, S., & Shao, L. (2014). Biomechanical properties of nano-TiO2 addition to a medical silicone elastomer: The effect of artificial ageing. *Journal of Dentistry. 42(4), 475-483.* doi:https://doi.org/10.1016/j.jdent.2014.01.002

Waters, M. G. J., Jagger, R. G., & Winter, R. W. (1996). Effect of surface modified fillers on the water absorption of a (RTV) silicone denture soft lining material. *Journal of Dentistry.* 24(4), 297-300. doi:https://doi.org/10.1016/0300-5712(95)00066-6

Watson S, Beydoun D, Scott J, Amal R (2004). Preparation of nanosized crystalline TiO2 particles at low temperature for photocatalysis. *Journal of Nanoparticle Research* 6(2): 193-207.

White, C., Tan, K., Wolf, A., & Carbary, L. (2010). In Dillard D. A. (Ed.), *4 - advances in structural silicone adhesives* Woodhead Publishing. doi:https://doi.org/10.1533/9781845698058.1.66

Willett, E. S., & Beatty, M. W. (2015). Outdoor weathering of facial prosthetic elastomers differing in durometer hardness. *Journal of Prosthetic Dentistry, 113*(3), 228-235. doi:10.1016/j.prosdent.2014.09.009 [doi]

Wypych, G. (2008). *Handbook of material weathering*. Elsevier.

Xie, J., Hu, J., Lin, X., Fang, L., Wu, F., Liao, X., Shi, L. (2018). Robust and anti-corrosive PDMS/SiO2 superhydrophobic coatings fabricated on magnesium alloys with different-sized SiO2 nanoparticles. *Applied Surface Science.* 457(1), 870-880. doi:https://doi.org/10.1016/j.apsusc.2018.06.250

Zayed, S. M., Alshimy, A. M., & Fahmy, A. E. (2014). Effect of surface treated silicon dioxide nanoparticles on some mechanical properties of maxillofacial silicone elastomer. *International Journal of Biomaterials, 2014*, 750398. doi:10.1155/2014/750398 [doi]

Zheng, Y., Zheng, Y., & Ning, R. (2003). Effects of nanoparticles SiO2 on the performance of nanocomposites. *Materials Letters,* 57(19), 2940-2944. doi:https://doi.org/10.1016/S0167-577X(02)01401-5

Zhuravlev, L. T. (2000). The surface chemistry of amorphous silica. Zhuravlev model. *Colloids and Surfaces A: Physicochemical and Engineering Aspects*, *173*(1-3), 1-38.

Zhuravlev, L. T., & Potapov, V. V. (2006). Density of silanol groups on the surface of silica precipitated from a hydrothermal solution. *Russian Journal of Physical Chemistry*, *80*(7), 1119-1128.